EFFECTS OF MICROSTRUCTURE ON HIGH-CYCLE FATIGUE OF AN AL-ZN-MG-CU ALLOY (AL-7055)

by

Lynn Eugene Oswald

BS Degree, Iowa State University, 1987

MS Degree, University of Pittsburgh, 2003

Submitted to the Graduate Faculty of

School of Engineering in partial fulfillment

of the requirements for the degree of

Master of Science

University of Pittsburgh

2003

UNIVERSITY OF PITTSBURGH

SCHOOL OF ENGINEERING

This thesis was presented

by

Lynn Eugene Oswald

It was defended on

April 15, 2003

and approved by

Anthony DeArdo, Professor
Department of Materials Science and Engineering

Ian Nettleship, Associate Professor
Department of Materials Science and Engineering

Thesis Advisor: Jorg M.K. Wiezorek, Assistant Professor
Department of Materials Science and Engineering

ABSTRACT

EFFECTS OF MICROSTRUCTURE ON HIGH-CYCLE FATIGUE OF AN AL-ZN-MG-CU ALLOY (AL-7055)

Lynn Eugene Oswald, MS

University of Pittsburgh, 2003

The study of fatigue in aluminum alloys is an area that has been studied for many years. Although proposed processes and mechanisms for fatigue initiation have been reported in various studies, there still exist areas that require improved understanding. The current study examines the role that microstructural features can play with regard to fatigue crack initiation.

Alloy 7055 has found wide acceptance by commercial aircraft manufacturers in the use of upper wing skins. This product displays a unique combination of compressive yield strength, fracture toughness and corrosion resistance which are required for use in compression-dominated upper wing structures. Fatigue crack initiation is used by aircraft designers to determine the initial inspection intervals an aircraft must adhere to. By increasing the fatigue initiation resistance of an aluminum alloy, an aircraft can endure additional flights prior to initial inspection. This has an obvious impact on the financial and safety performance of the structure.

Constituent particles (Mg_2Si and Al_7Cu_2Fe) play a primary role in the fatigue crack initiation resistance of 7055 alloy. In the current study Mg_2Si was determined to be a particularly damaging feature in the microstructure in terms of fatigue crack initiation resistance, as compared to Al_7Cu_2Fe. The elastic and plastic behavior of these particles, as determined with an atomic force microscope (AFM) equipped with a nanoindenter, revealed that the Fe-bearing particles were more resistant to fracture and exhibit increased plasticity, as compared to the Si-bearing particle.

PREFACE

The opportunity to complete this thesis project was due in large part to the encouragement of Kent Young and Dr. John Liu, to whom I would like to express my gratitude. After working in an aluminum production facility for more than twelve years, I was given an opportunity to obtain a Master of Science degree, which has been a personal goal since undergraduate school. This experience has been most valuable, and will provide additional tools and skills that will better prepare me for the challenges that lie ahead in my career. In addition, my advisor, Dr. Jorg Wiezorek, has been very helpful in guiding me in the right direction and challenging me to reach to a higher level. For this guidance, I am very appreciative.

As I leave the research environment and return to the production environment, I reflect upon the experience, which has been bestowed upon me, and I realize, I am very fortunate to have been given an opportunity to gain this experience. I have been able to work alongside the technical experts in their respective fields, and the friendships and contacts that have been established will be with me forever. I am confident I will be able to fulfill the supportive comments of my former colleagues which were written on a plaque given to me during my departure which stated: “May you return with the knowledge of the Masters”.

On a personal level, this experience has been challenging and rewarding for my family also. My wife, Melody, and children, Amanda, Emily, Andrew and Sarah left a very comfortable and stable environment to allow me to pursue this opportunity. I am eternally thankful to them for their sacrifice; however, I also know that we will all look back at this experience with a multitude of happy memories. This has been an experience that has broadened all of us, and we have become a tighter-knit family as a result of this time in the Pittsburgh area. I want to especially thank Melody for her support and encouragement during this process, as she has been the steadfast foundation that has kept our family on track during the past two years.

TABLE OF CONTENTS

LIST OF TABLES

LIST OF FIGURES

1.0 INTRODUCTION

1.1 Introduction

Alloy Al-7055 is a member of the family of age hardenable Al-Zn-Mg-Cu alloys (Al-7xxx series, in which Zn is the major alloying element), which, due to the high yield strength that can be achieved, are used in aerospace applications for structural components. Al-7055-T7751[1] is a plate product that was developed for upper wing products used in commercial aircraft to provide the same as, or higher compressive yield strength than a –T6 temper (peak strength), with improved fracture toughness and corrosion resistance. The compressive yield strength levels need to be kept as high as possible, since the application is compression dominated. On the other hand, fracture toughness and corrosion resistance are also important properties, since the structures that this product is used with must resist fracture and exhibit resistance to aggressive, aqueous environments. Increasing the fatigue resistance is an interesting technological challenge, and becomes important from a performance standpoint, since the initial inspection intervals are dictated by the product's ability to resist crack initiation and growth. The fatigue crack growth resistance of a material determines subsequent inspection intervals.

Al-7055-T7751 plate is produced by the following processing steps: vertical direct chill ingot casting, homogenization thermal treatment, hot rolling in an aluminum reversing mill at ~$0.9T_m$, solid solution heat treatment and quench, stretching to remove residual stresses caused by quenching, and finally, artificial aging to achieve the desired strength and fracture toughness properties. During the solidification process of the ingot casting, several constituent particles are formed, some of which are strengthening phases that are dissolved upon further processing (during homogenization, solution heat treatment and artificial aging), while some remain in the solid state all the way to the finished product. Two of the latter type of constituent particles that are insoluble after casting are Al_7Cu_2Fe and Mg_2Si. These particles can be particularly detrimental from a fatigue property standpoint. This issue will

[1] -T7 temper applies to solution heat-treated and overaged/stabilized wrought products that are beyond peak strength to provide, in this case, increased corrosion resistance and fracture toughness. The –T_51 designation implies a 1.5% to 3% stretching operation after solution heat treatment. Source: Aluminum Standards and Data 2000, The Aluminum Association.

be further investigated and documented in this study. The current approach to minimize the presence of these phases is to reduce the level of Fe and Si in the initial melt.

Failure by high cycle fatigue is broken up into three distinct regimes: crack initiation, short crack growth and long crack growth. A large portion of the service life of aerospace products is spent in the crack initiation and short crack growth regions of the total fatigue life of a component. A recent report has shown that initiation and small crack growth can represent 50 to 90 percent of the total fatigue life.[1] Thus, it is necessary to understand the important microstructural features that control crack initiation. A stress-life (S/N) curve, also known as a Wöhler diagram (named after August Wöhler, who performed fatigue research in the 19th century)[2], is often used to compare the fatigue initiation resistance of engineering materials. As the magnitude of the applied stress (S) is decreased, the number of cycles to failure (N) increases for metallic alloys. If a sufficiently low stress is applied and failure does not occur within a prescribed large number of cycles (e.g. 10 million), the material is said to have reached its endurance limit. The endurance limit scales with the yield stress of the material.[2]

There are two design philosophies employed by aerospace engineers, in order to determine the operating lives for aluminum-based aerospace alloys: damage tolerance and safe-life.[3] In the damage tolerance methodology, which is the current approach used in the commercial aircraft industry, S-N fatigue performance dictates initial inspection intervals for all four major aluminum aerospace products (fuselage, upper wing, lower wing and spars/ribs - i.e. thick plate). For repeat inspection intervals, however, fatigue crack growth and fracture toughness properties are the primary property factors. The damage tolerance approach for commercial aircraft assumes that a flaw already exists in a critical part, but this flaw will remain below a critical size during the planned service life of the structure. This has proven to be an effective method of ensuring safe lives for critical structures, as long as the proper inspection procedures are followed.

In the case of the safe-life philosophy, which was abandoned in about 1970, a full-scale ground-fatigue test article of a production aircraft was used to set the “safe-life” of a structure. The design life was then selected as ¼ of the life demonstrated in this test article. This approach assumed that the structure was initially flaw-free, and a factor of safety of 4, combined with regular in-service inspections, would detect any flaws before they became

catastrophic. Since flaws are present in any structure (due to manufacturing practices, material production and environmental conditions) - this approach was not adequate to ensure planned lifetimes were met. Several examples have been described by Tiffany[4], where catastrophic failures in United States Air Force aircraft occurred before one lifetime, as determined by the safe-life approach, of the structure was reached. Hence, the damage tolerance approach is clearly the better design philosophy.

With many new airframe structures being manufactured with monolithic structures, resistance to fatigue initiation becomes increasingly important. A monolithic structure does not have the inherent crack-arresters that exist in a built-up structure, which consists of many separate parts that are joined together by various fastening techniques. For example, the wings of commercial aircraft traditionally use a plate wing skin that is riveted to an extruded stringer. Since the structure is not monolithic, a crack advancing in the wing skin is more likely to stop when it reaches the extruded stringer than in the case of an integral structure. Monolithic structures are becoming more attractive due to the advent of high speed machining, which has significantly driven down the total cost of manufacturing. The traditional structures have been built up, using rivets and other joining techniques, but they employ many more parts and are considerably more labor intensive to construct. Thus, development of detailed understanding of processing-microstructure-property relationships related to fatigue initiation is very important and timely.

For thick plate products (4" – 8"), crack initiation sites have been observed at micropores that are present in the ingot, and formed during solidification.[5] Hot rolling variables can be manipulated to "heal" these micropores, and ultimately improve the fatigue lives of the plate. Large open pores appear to be more detrimental on fatigue performance than small slender pores, even though their maximum dimensions are the same.[5] For thinner plate products (less than 4") - the residual micropores that are remaining from the solidification process are typically healed during hot rolling, due to the compressive rolling stresses. In the hierarchy of microstructural features that are likely to lead to crack initiation, constituent particles are the next microstructural inhomogeneity that is likely to initiate cracks.

Models have been developed to predict evolution of fatigue damage in precipitation strengthened Al-alloys starting from inherent microstructural feature populations.[6] Intrinsic

microstructural features that have been associated with crack initiation sites include constituent particles, dispersoids, precipitates, inclusions, pores, grain boundaries, precipitate free zones (PFZ's), persistent slip bands and texture.[7] The effect of these features on the fatigue performance can, in some cases, be altered by way of alloy composition modifications and thermomechanical processing (TMP). However, there is currently no methodology for assessing "a-priori" the impact these changes have on preventing the development of widespread fatigue damage.[7] The role of the crack initiation sites in the fatigue process will be discussed in the following section.

1.2 Crack Initiation Sites

Constituent particles are insoluble phases that form during the direct chill (DC) solidification process. In the case of 7055 alloy, there exist two such phases: Al_7Cu_2Fe and Mg_2Si. During solidification, Al_7Cu_2Fe is the first phase to form at 1078° F (581° C), while Mg_2Si forms at 924° F (496° C).[8] Since subsequent thermal operations are well below these temperatures (less than 900° F (482° C)), these two phases remain as insoluble constituent particles in the aluminum matrix throughout the remaining processing steps. These particles can be as large as 30 μm in the longest direction.[9] The particles can be strung out and broken up during rolling, but once they are formed, cannot be dissolved in solid solution. The quantity, size, and distribution of these particles can be a factor in the role they play in the fatigue process. Recently S/N fatigue data has been generated to illustrate that decreasing the amount of Fe and Si that is present in the melt will increase the fatigue lifetimes at equivalent stresses (e.g. Figure 1).[10] It is clear from Figure 1 that the alloys with reduced Fe and Si content (Imp 7055, full symbols in Figure 1) larger maximum and average number of cycles to failure than standard alloys (Std 7055, open symbols in Figure 1).

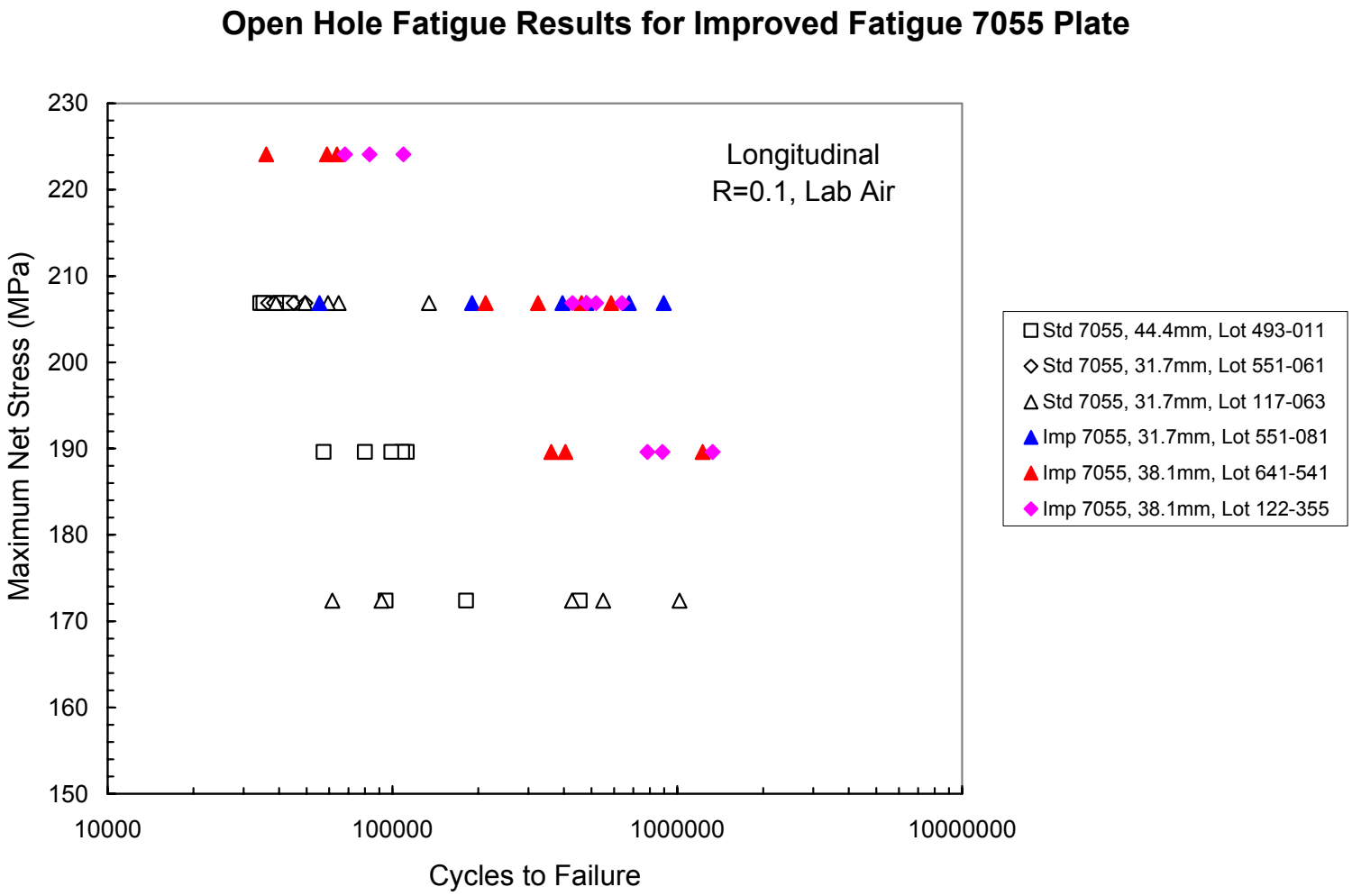

Figure 1 Open Hole Fatigue Results Comparing Standard and Improved Fatigue 7055 Plate

Aside from reducing the amount of Fe and Si in the alloy, very little can be done to reduce the effect of these constituent particles in fatigue initiation for ingot metallurgy. This is primarily due to the thermodynamically favorable formation of the large Fe and Si bearing constituents mentioned above. A study comparing gas atomized solidification from the melt, which resulted in much higher solidification rates than standard ingot metallurgy, revealed that fatigue performance could be improved, even with high volume fractions of Fe and Si.[11] The reasons for the improvement are due to the formation of a finer grain size and the Fe and Si particles are of a much smaller size, as compared to ingot metallurgy.

Dispersoids are another type of intermetallic particle that can form by solid state precipitation. These particles are added to aluminum alloys to suppress recrystallization in a hot worked structure. Typically, up to 0.3% Cr, 0.8% Mn or 0.15% Zr are added to the melt to precipitate out during thermal processing. The Cr particles ($Al_{12}Mg_2Cr$) and Mn particles ($Al_{20}Mn_3Cu_2$) are relatively large (roughly 0.02 to 0.5 μm in the longest direction), while the Zr particles ($ZrAl_3$) are much smaller (less than 0.01 μm in the longest direction).[9] Due to size compatibility the Zr particles are coherent with the aluminum matrix, while the Cr and Mn particles are incoherent. The current alloy being studied (7055) utilizes Zr as the dispersoid forming particle.

Precipitates are another type of microstructural feature that develops during artificial aging. For 7xxx series alloys, the overaged, -T7x tempers are employed to improve the corrosion resistance and fracture toughness of the material. In the case of 7055 alloy, the sequence of precipitate transformation is G-P zones – η' (transition precipitates) – η (equilibrium precipitates). These equilibrium precipitates are non-shearable particles that promote homogenous deformation through Orowan-type dislocation looping or bypassing of the precipitates, which improves the fatigue initiation characteristics of the material.

Grain boundaries have been shown to have an effect on short crack growth, with fine grain size being more resistant to short crack growth. Since a transgranular fatigue crack can initiate along a localized slip band, which is induced by a stress concentration, the grain boundaries will act as a barrier to inhibit the growth of a crack. If the grains are large, a transgranular crack can travel a greater distance before potentially being stopped or deviated by encountering a grain boundary. If a crack reaches a critical length, such that the crack no

longer is stalled at the grain boundary, the crack growth rate becomes smooth and the crack is no longer impeded by the grain boundaries.

Precipitate free zones (PFZ's) are vacancy-depleted regions adjacent to a grain boundary decorated by precipitates (e.g. η in 7xxx alloys). PFZ's are the result of preferential nucleation of precipitates at a grain boundary, due to the boundary lowering the surface and strain energies of the precipitates. Since the zones are depleted of solute, they will be mechanically weaker than the matrix, which can create strain localization, and consequently may lead to crack nucleation. In the presence of a PFZ, a material containing a fine grain size will exhibit longer fatigue lives than a large grain material. This is attributable to the increase in the number of cycles required for fatigue initiation in the fine grained material. Since the fine grain material has a shorter slip distance, the local stress concentration will be reduced, and fewer cracks will nucleate.[12]

PFZ's have been shown to have an impact on fatigue properties.[12] One study has shown that the ratio of grain boundary precipitate size (d) to the width of the PFZ (w) can be used as a parameter to describe the resistance of the material to intergranular fracture.[13] Namely, when d/w is large, the properties of the grain interior are the dominant factor, whereas, when d/w is small, the PFZ properties determine the intergranular fracture resistance. For this product, a typical value of d is 40 nm, while a typical value of w is 50 nm, resulting in a d/w ratio of 0.8. This is considered to be the lower-bound value.[14] Therefore, in order to improve fatigue initiation resistance, it is important to minimize the size of grain boundary precipitates as well as the width of the PFZ.

HCP (e.g. titanium) structures exhibit anisotropic elastic modulus values depending upon the crystallographic orientation. Therefore, a short crack will frequently stop or change directions whenever a grain boundary is encountered. Aluminum (FCC), on the other hand, displays an almost perfectly isotropic elastic modulus and has a greater number of available slip systems. For this reason, crystallographic orientation does not affect as strongly as in the anisotropic Ti the fatigue strength in aluminum alloys. A preferred crystallographic orientation can, however, cause a change in the crack growth direction after initiation, which becomes more important when considering fatigue crack growth testing. Studies have shown a 3-6 ksi (21-41 MPa) improvement in several cases by this texture-related mechanism.[15, 16, 17]

2.0 OBJECTIVES OF STUDY

The main objective of this study is the investigation of the effects of the hierarchical microstructural features on the high cycle fatigue performance of Al-7055-T7751 plate material that has been processed under realistic commercial production conditions. More specifically, here the effects of the microstructural variations typically encountered in Al-7055 plate as a function of depth position and lateral location in the plate have been studied. Hence, in the current project, fatigue specimens were extracted from the edge and center sections of plate material as well as through the thickness, t, at three locations (surface, t/4 and t/2, where t is the plate thickness). Since the center of the ingot is the last to freeze during solidification, this is where the largest constituent and other intermetallic particles are expected to be located. However, this is also the location which contains the lowest level of solute (due to macrosegregation). Conversely, the t/4 location contains the highest level of solute, also due to macrosegregation during solidification.

High cycle fatigue tests (sheet type and round bar) have been performed to establish stress-life data as a function of location within the plate. The microstructures have been studied by optical light and scanning electron microscopy together with texture measurements by X-ray diffraction. Mechanical properties have been determined by tensile tests and locally by nanoindentation with a specialized atomic force microscope. Through correlation of microstructure-property relationships, an assessment of the roles of the various hierarchical microstructural features on fatigue life with a focus on initiation has been attempted.

3.0 EXPERIMENTAL PROCEDURE

3.1 Material and Processing

The product chosen for this study was a 0.97" thick 7055-T7751 wrought plate item that was produced using standard production thermomechanical processing (TMP). This alloy-temper was chosen because of its extensive use in current and future commercial aircraft upper wing structures. The lot number of the material was 448-392. The plate material was hot rolled from a 16" thick vertical direct chill (DC) ingot that was cast 60" wide. The ingot was scalped, homogenized, and hot rolled to finish thickness on a hot reversing mill. During rolling, the ingot was broadened enough to meet a 90" wide finished width specification. The plate was then solution heat treated, stretched and aged to the final temper and specimens were extracted from the finished plate for testing. The composition (in weight percent) of the material is shown below in Table 1.

Table 1 Alloy Composition in Weight Percent (wt. %)

Alloy 7055									
	Si	Fe	Cu	Mn	Mg	Cr	Zn	Ti	Zr
AA Limits	0.10	0.15	2.0-2.6	0.05	1.8-2.3	0.04	7.6-8.4	0.06	0.08-0.25
As Tested	0.077	0.112	2.42	0.006	1.93	0.001	8.08	0.022	0.12

3.2 Fatigue Testing:

Two types of fatigue specimens were tested in this study: 1) A 0.100" thick flat specimen to measure the fatigue lives through the thickness (near-surface, t/4 and t/2); 2) A smooth round specimen (diameter = 0.3") centered at mid thickness (t/2). All fatigue tests were performed at room temperature with a stress ratio, R=+0.1, at a frequency of 25 Hz. Both specimens were polished to a smooth finish to minimize the chance of having a stress riser on the surface, which could have an effect on the fatigue test results.

3.3 Atomic Force Microscopy (and Nanoindentation):

In an effort to understand the elastic and plastic behavior of the Al_7Cu_2Fe and Mg_2Si constituent particles, as well as the aluminum matrix, a Digital Dimension 3000 atomic force microscope (AFM) equipped with an automated Hysitron Triboscope was utilized to measure the resistance to indentation with varying loads. The maximum load was adjusted to obtain a maximum indentation depth of approximately 300 nm, with eight successive indentations being utilized to calculate the hardness and reduced modulus of each microstructural feature.

3.4 Texture Measurements – X-ray Diffraction:

Pole figures and orientation distribution functions (ODF) were determined utilizing x-ray diffraction for various specimens representing through-thickness and across-width locations. The texture samples were initially machined to 6.35 mm (0.25”), and then chemically etched to 0.1 mm (0.004”) thick to remove any cold working effects from machining. The rolling direction on the specimens was aligned with the rolling direction on the pole figures. The equipment used for this determination was a Rigaku Geigerflex, using monochromatic Cu radiation ($\lambda = 1.54439$ Å). The ODF was calculated from three pole figures that were collected from each specimen.

3.5 Scanning Electron Microscopy (SEM):

A Phillips Field Emission Gun - Scanning Electron Microscope (FEG-SEM), equipped with an energy dispersive spectrometer (EDS), was used to analyze fatigue initiation sites, and determine the composition of the initiation sites. Both secondary and back-scatter electron (SE and BSE) imaging modes have been employed.

3.6 Optical Microscopy (OM):

Specimens were polished and etched in a solution of Kellers etch to reveal the grain structure and degree of recrystallization.

4.0 RESULTS AND DISCUSSION

In an effort to determine the variation in fatigue performance across the width, down the length, and through the thickness of a plate, a lot of 1" thick 7055-T7751 rolled plate was chosen from a standard processed hot rolled material. This plate was then subjected to axial fatigue testing to failure using the two different types of specimens previously mentioned. The results of the axial fatigue tests are shown in Figure 2 and Figure 3 on the following page. In both specimen types, the fatigue lives for the edge specimens were clearly longer than those for the center specimens. The maximum stress was kept constant at 45 ksi for the flat specimen type, and has been slightly separated in Figure 3 for clarity.

Several techniques were employed in an effort to discern the differences in the fatigue performance of the material. These include: 1) statistical analysis of the data, 2) energy dispersive spectroscopy (EDS) analysis of the fatigue initiation sites, 3) atomic force microscope (AFM) equipped with a nanoindenter, and 4) texture analysis. The results of these investigations are described in the following section.

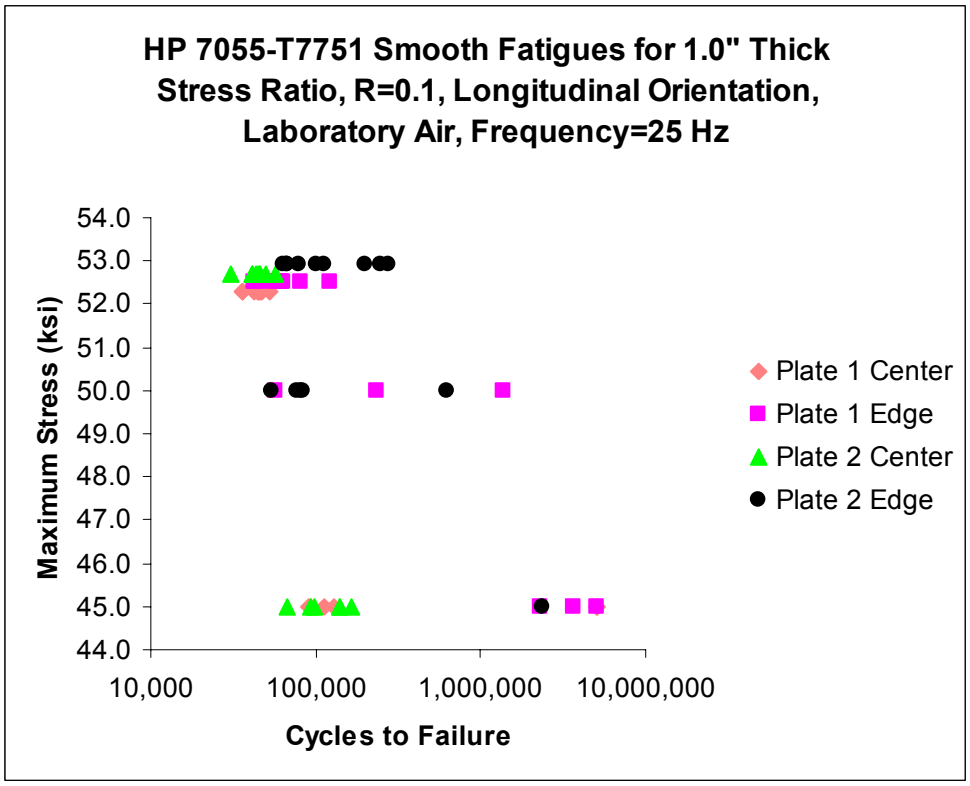

Figure 2 Round Bar Fatigue Results Comparing Plate Center to Edge Location

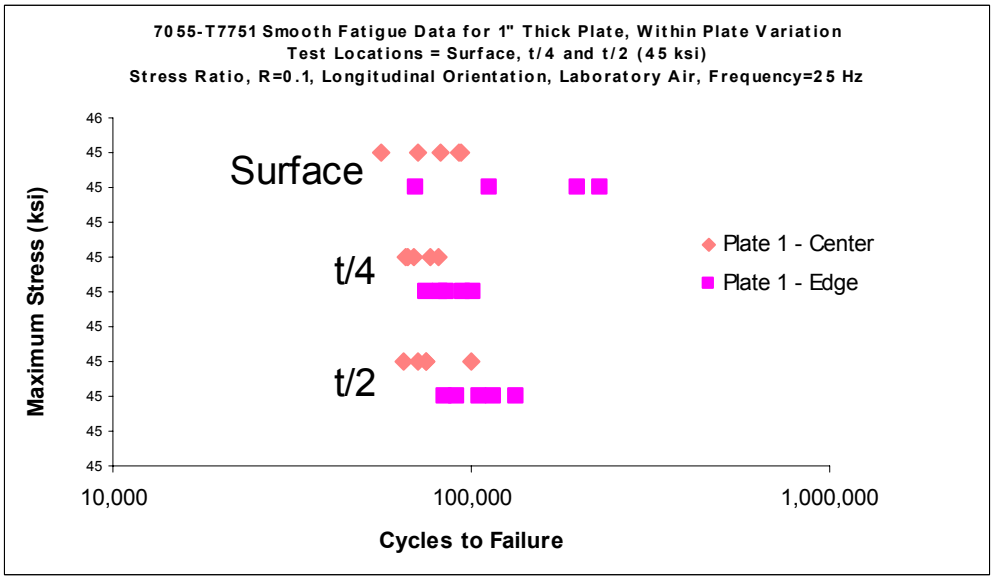

Figure 3 Flat, Sheet-type Fatigue Specimen Comparing Through-thickness Fatigue

4.1 Statistical Results

The statistical analysis for the flat specimen type revealed that the fatigue test performances of the edge and center locations were not statistically different. The results of these tests are displayed in Figure 5. For the round specimen type, the maximum stress was varied between 45 and 52.5 ksi, and the results are shown in Figure 2. A statistical analysis was performed to determine if the differences in fatigue performance were statistically significant and/or important for the latter. The most revealing observation was that at the lower stress levels, the edge specimens exhibited much higher fatigue lifetimes. However, at higher stresses, the lifetimes for the edge and center were quite similar (see Figure 2). This is shown graphically in Figure 4, which predicts that the edge specimens should exhibit a fatigue life that is nine times longer than that of the center specimens at a stress level of 45 ksi. At the higher stress level of 52.5 ksi, the graph indicates expected fatigue lives for the edge specimens only about twice as long as for the center specimens. Hence, the difference in fatigue lives for the round specimen tested at different stress levels was found to be statistically significant.

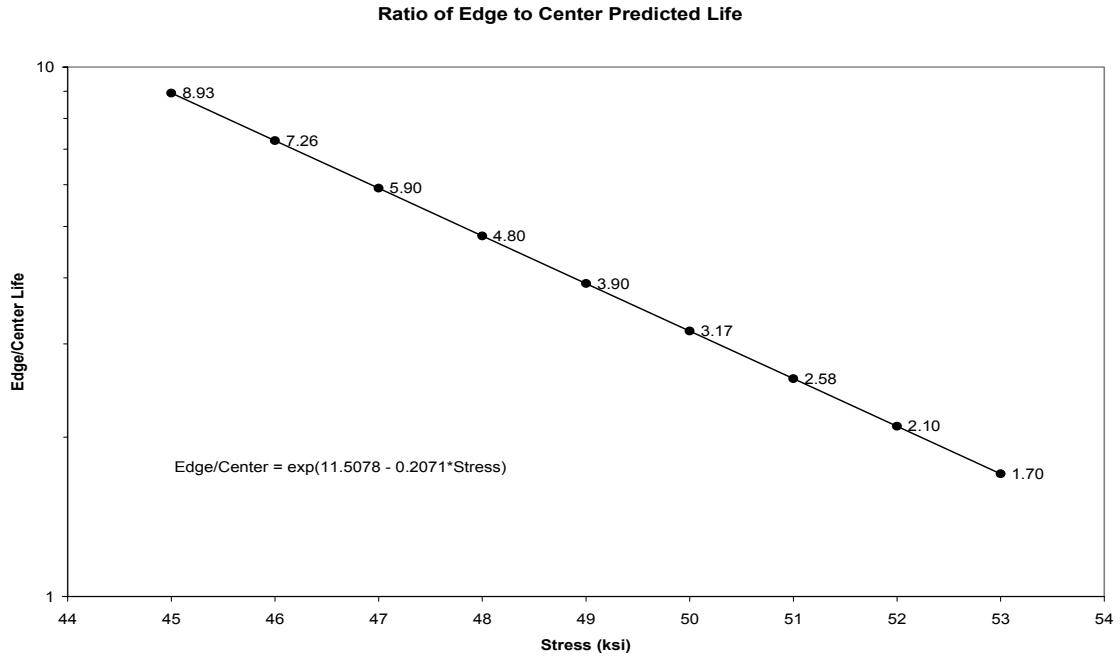

Figure 4 Predicted Lifetimes Showing Increased Probability of Edge Specimens Exhibiting Higher Lifetimes Than Center Specimens, Especially at Lower Stress Levels

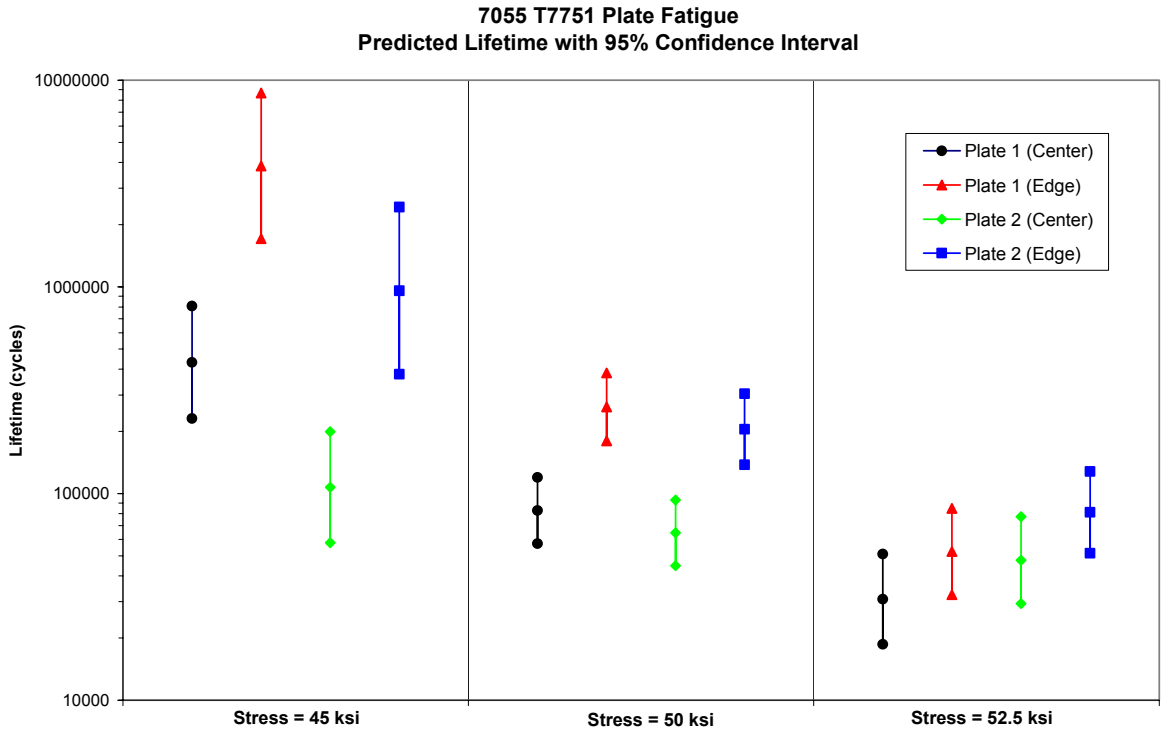

Figure 5 Graphical Representation of Statistical Analysis, With 95% Confidence Intervals

4.2 Light Optical Microscopy

In an effort to determine whether microstructural differences between edge & center and through-thickness locations of the Al-7055 plate could be discerned optically that might be suitable to explain the observed fatigue performance differences, optical microscopy has been performed. The main differences between the edge and center investigated here were grain size, grain morphology and degree of recrystallization.

The optical photomicrographs shown in Figure 6 display the microstructural differences that exist between the edge and center specimens, as well as through the thickness of the plate. Near the surface, the grains are elongated and nearly completely recrystallized. As the depth profile is increased, the amount of recrystallization gradually decreases, and near the mid-plane becomes nearly completely unrecrystallized. However, upon comparing the edge to center specimens, there are no discernible differences in grain structure. Therefore, the observed edge-to-center fatigue performance differences cannot be attributed to significant grain structure differences.

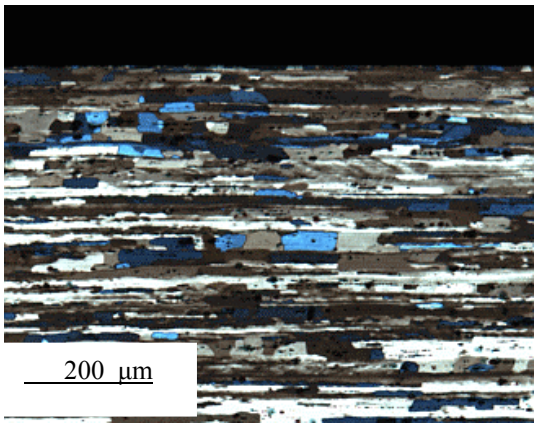

Plate Edge – Top surface

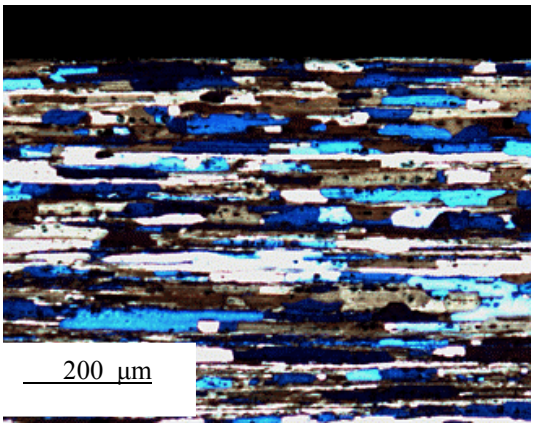

Plate Center – Top surface

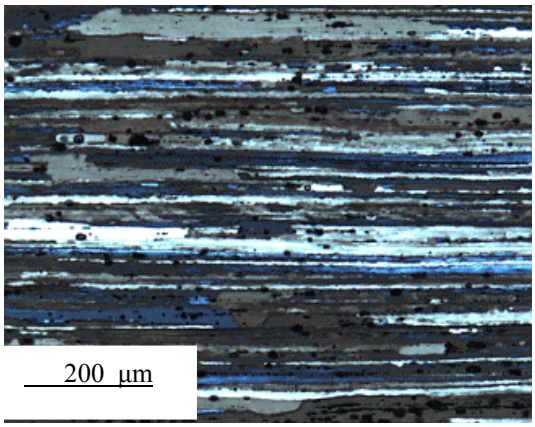

Plate Edge – 0.2” below top surface

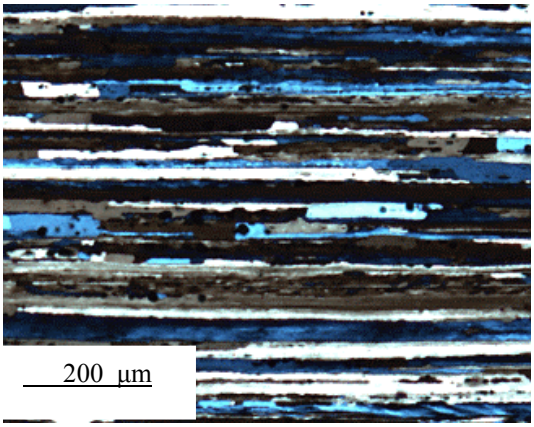

Plate Center – 0.2” below top surface

Figure 6 Photomicrographs showing microstructures at and near the plate surface

4.3 X-Ray Diffraction - Texture and Orientation Distribution Function

Texture is defined as a preferred crystallographic orientation of grains in a polycrystalline material [18]. Here two methods of experimental texture measurement were employed: 1) pole figure determination, and 2) the orientation distribution function (ODF). A pole figure is a graphical polar projection which displays the distribution of crystallographic orientations for a given plane [19]. The baseline is a completely random specimen that is typically prepared by sintering a powder of the material that is being measured. The pole density output is then reported in terms of the intensity of "times random".

Texture measurements were performed on selected specimens from both the edge and center specimens, through the thickness, to determine if preferred grain orientation might be playing a role in the fatigue life differences. The texture analysis revealed that a shear texture exists near the surface, while a plane strain, or hot rolling type texture exists near the mid-thickness, which is the expected texture from a hot rolled 7xxx alloy plate material. Additionally, the pole figures indicated that the textures near the edge and center of the plate were similar for a given through-thickness location. For brevity, in Figures 7 – 9, pole figures representative of through-thickness locations from near the edge and center of the plate are compared. The maps of ODF and additional pole figure data are collated in Appendix A.

Based on the quite strong similarities in texture between the edge and center specimens (Figure 7 – 9, and see Appendix A), the level of preferred orientation cannot be responsible for the consistently higher fatigue lives of the edge specimens with respect to those of the center specimens.

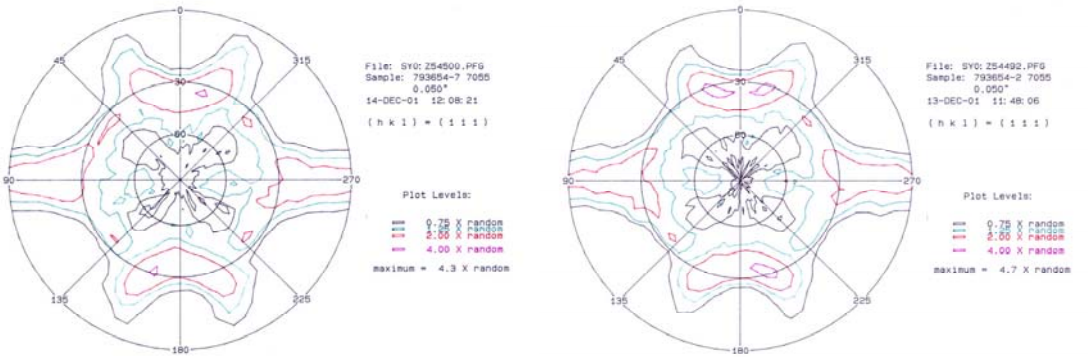

Figure 7 Pole figures for edge (left) and center (right) specimens, machined at t=0.050”

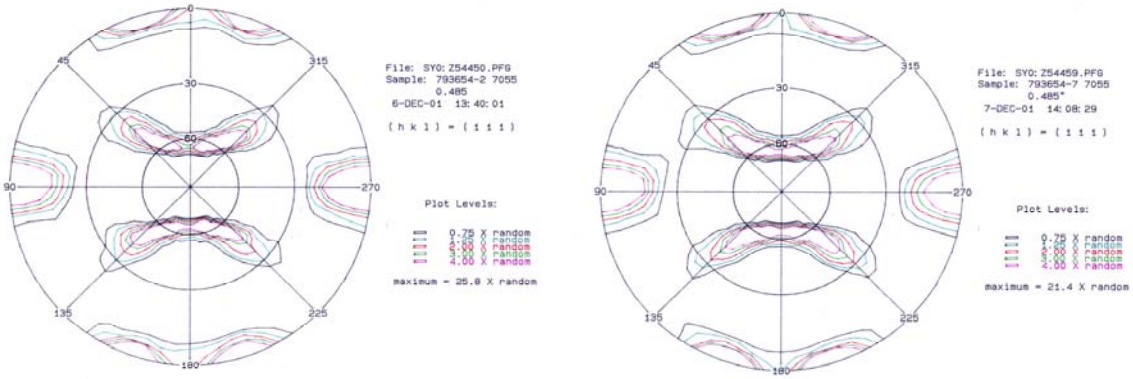

Figure 8 Pole figures for edge (left) and center (right) specimens, machined at t=0.485”

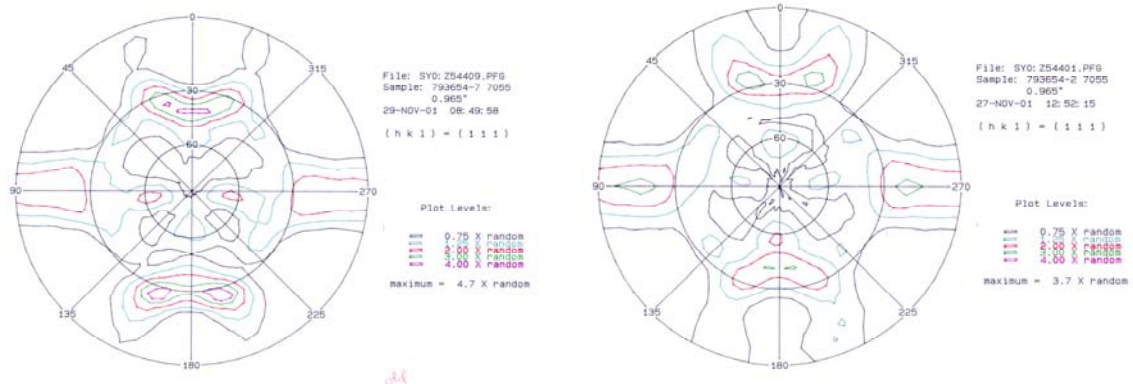

Figure 9 Pole figures for edge (left) and center (right) specimens, machined at t=0.965”

4.4 SEM - Analysis of Fatigue Crack Initiation Sites:

The fatigue crack initiation sites have been investigated of the flat specimens in a field emission gun scanning electron microscope (FEG SEM), utilizing imaging techniques and energy dispersive x-ray spectroscopy (EDS) analysis. The results of those analyses are shown in Table 2. With the exception of three of the specimens, the crack initiation sites were determined to be either Mg_2Si or Al_7Cu_2Fe constituent particles. These particles cannot be dissolved in 7xxx aluminum alloys during heat treatments after casting. The silicides appear to be particularly effective initiation sites. Usually samples with crack initiation sites associated with Mg_2Si particles exhibit shorter fatigue lives (smaller number of cycles to failure) than those with initiation sites associated with Fe-containing particles.

Table 2 Lifetimes and Initiation Sites for Through-thickness Fatigue Specimens

Location	Spec. ID	Max. Stress	N	Initiation Site	Apparent Size (μm)	Surface/Interior	Comments
surf-0.120	1-2E L7	45	70128	Mg_2Si	18.5 x 5.5	Surface	
	1-2E L13	45	228628	Al_7Cu_2Fe	29.4 x 14	Surface	
	1-2E L10	45	199144	Al_7Cu_2Fe	182 x 45.9	Surface	
	1-2E L1	***50***	62150	Mg_2Si	42.9 x 10.5	Sub-Surface	4.5 μm (σ = 50 ksi, all others = 45 ksi)
	1-2E L4	45	112518	Mg_2Si	15.3 x 6.5	Surface	C, S, Cl, K also (Salt debris)
t/4	1-2E L14	45	82112	Mg_2Si	5.7 x 13.1	Sub-Surface	3 μm
	1-2E L11	45	85147	Al_7Cu_2Fe	43 x 29.7	Surface	
	1-2E L5	45	95305	Mg_2Si	19.1 x 17.2	Sub-Surface	8.7 μm - C, S, Cl, K also (Salt debris)
	1-2E L2	45	101807	Al_7Cu_2Fe	93.7 x 19.9	Sub-Surface	1.9 μm
	1-2E L8	45	75268	Al_7Cu_2Fe	19.7 x 10.4	Surface	
t/2	1-2E L9	45	84145	N/A	N/A	Surface	Mechanical Damage - Sample Prep.
	1-2E L6	45	91678	Mg_2Si	15.5 x 11.2	Sub-Surface	10 μm
	1-2E L12	45	105224	Al_7Cu_2Fe	3.2 x 6.8	Surface	Salts (Bright particles - Ca)
	1-2E L15	45	116278	Mg_2Si	2.8 x 2.1	Surface	
	1-2E L3	45	133972	Mg_2Si	16.3 x 10.8	Sub-Surface	
surf-0.120	1-2C L10	45	55694	Mg_2Si	6.6 x 5.3	Sub-Surface	1 μm
	1-2C L13	45	82452	Mg_2Si	7.5 x 5.3	Sub-Surface	1.8 μm
	1-2C L7	45	92696	Mg_2Si	23.8 x 11.7	Surface	
	1-2C L1	45	93474	Mg_2Si	20.4 x 8.9	Surface	
	1-2C L4	45	71131	Al_7Cu_2Fe	15.2 x 9	Sub-Surface	9.8 μm - Void
t/4	1-2C L2	45	66523	Mg_2Si	11.4 x 6.2	Surface	
	1-2C L5	45	77032	Mg_2Si	10.9 x 3.3	Surface	
	1-2C L8	45	80782	Al_7Cu_2Fe	15.8 x 10.4	Surface	
	1-2C L11	45	65607	Mg_2Si	6.1 x 4.1	Sub-Surface	1.5 μm
	1-2C L14	45	68977	Stage I	N/A	Surface	Matrix only - Stage I
t/2	1-2C L15	45	99463	Mg_2Si	30.7 x 13.1	Surface	
	1-2C L3	45	75067	Mg_2Si	35.2 x 11.3	Surface	
	1-2C L6	45	74546	Mg_2Si	22.4 x 7.2	Surface	
	1-2C L9	45	64824	Mg_2Si	33.4 x 12	Sub-Surface	1 μm
	1-2C L12	45	71371	Mg_2Si	17.6 x 11.5	Surface	

As can be discerned from Table 2, the "apparent" size of the constituent particle does not alone explain the reason for the particle being the source of the initiation site. A larger "apparent" particle size does not necessarily lead to a short fatigue life. This could be due to the fact that the particle is a three dimensional object, and the apparent size of the particle viewed in the microscope may not be indicative of the maximum dimensions of the particle. The orientation of the particle relative to the matrix, as well as the morphology of the particle will also determine its ability to resist fatigue initiation. If a constituent particle is oriented such that it lies in a slip plane, dislocations could pile up around the particle, and eventually lead to crack initiation. In addition, if a particle has sharp edges or is cracked from previous processing (stretching or rolling), it could act as a stress-riser, and lead to the preferential initiation of a crack.

Constituent particles are of dimensions on the order of μm, while a slip plane is a crystallographic plane, i.e. of dimensions on the order of 10^{-4} μm. Hence, just about any constituent particle will be of sufficient size to act as a stiff, hard obstacle for propagation of glide dislocations in a slip plane. Differently oriented aluminum matrix grains deform during the fatigue loading by activation of slip systems <uvw> {hkl}. Some grains are favorably oriented and have only one highly stressed active system, while others may be oriented such that a number larger than one of slip systems experience resolved stresses of about equal magnitude. In the latter case, a pile-up of dislocations against a constituent particle could possibly be less damaging than in the former. The pile-up stress locally reaches a critical value, which when it exceeds a resolved critical shear stress on an appropriately oriented slip system of the matrix will activate glide of dislocations of this system and thus dissipates the pile-up stress, preventing further rise in local stress. If no slip system is oriented favorably, the pile-up stress may continue to rise to levels sufficient to produce a crack at the interface or in the presumably brittle constituent particle.

Electron photomicrographs of the Mg_2Si and Al_7Cu_2Fe constituent particles are shown in Figures 10 through 15. Figure 10 shows an Mg_2Si particle at an initiation site, while Figure 11 shows the same Si-bearing particle at much higher magnification (15,000X). These photomicrographs illustrate the brittle nature of the fracture of the Si-bearing particles, showing a very clean, cleaved surface through the particle. Figures 12 and 13 show typical Al_7Cu_2Fe particles at the initiation site of a fatigue specimen. These particles, like the Si-

bearing particles, are usually located at or near the surface of the broken fatigue specimen if they acted in association with crack initiation. However, the Fe-bearing particles appear to exhibit very different fatigue behavior than the Si-bearing particles. Close observation of Figure 14 and Figure 15 illustrate this point very well. These two photomicrographs display the same Fe-bearing particle, with Figure 14 being taken at 5,000X magnification, and Figure 15 being taken at 15,000X magnification. In the highlighted, left-central area of Figure 15, the region of the striated particle can be observed. Based on this observation, one may be tempted to conclude that the Fe-bearing particle is capable of some plasticity and thus of accumulating a larger number of fatigue cycles prior to breaking, and ultimately initiating a crack. This will be explored in the next section, whereby an atomic force microscope, equipped with a nanoindenter was used to measure the modulus and hardness of the Si-bearing and Fe-bearing particles. In order to explore this interesting possibility, atomic force microscopy combined with nanoindentation has been performed to measure locally the hardness and elastic properties of the constituent particles (see section 4.6).

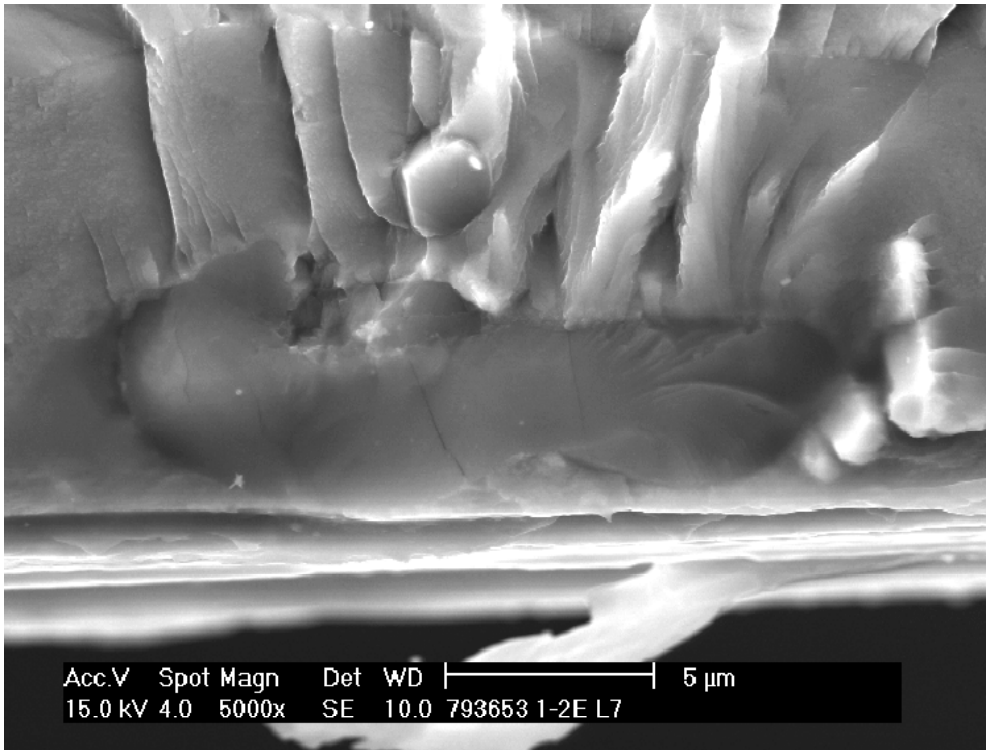

Figure 10 Mg_2Si particle at the fatigue initiation site

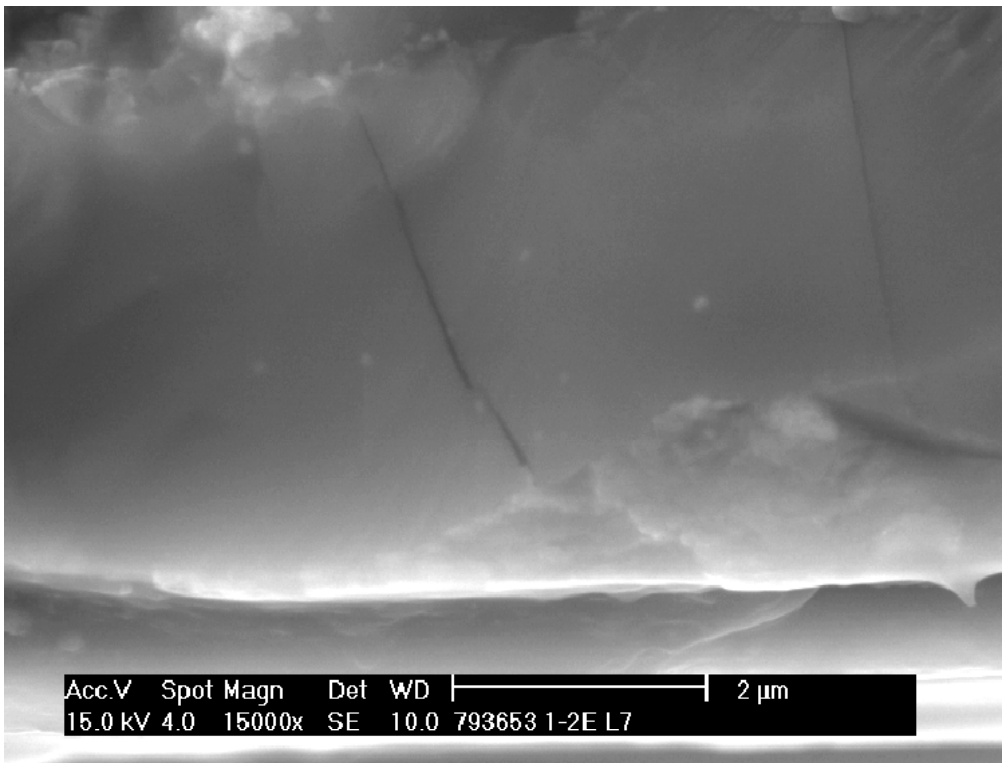

Figure 11 Same Mg_2Si particle showing close-up of crack running through the particle

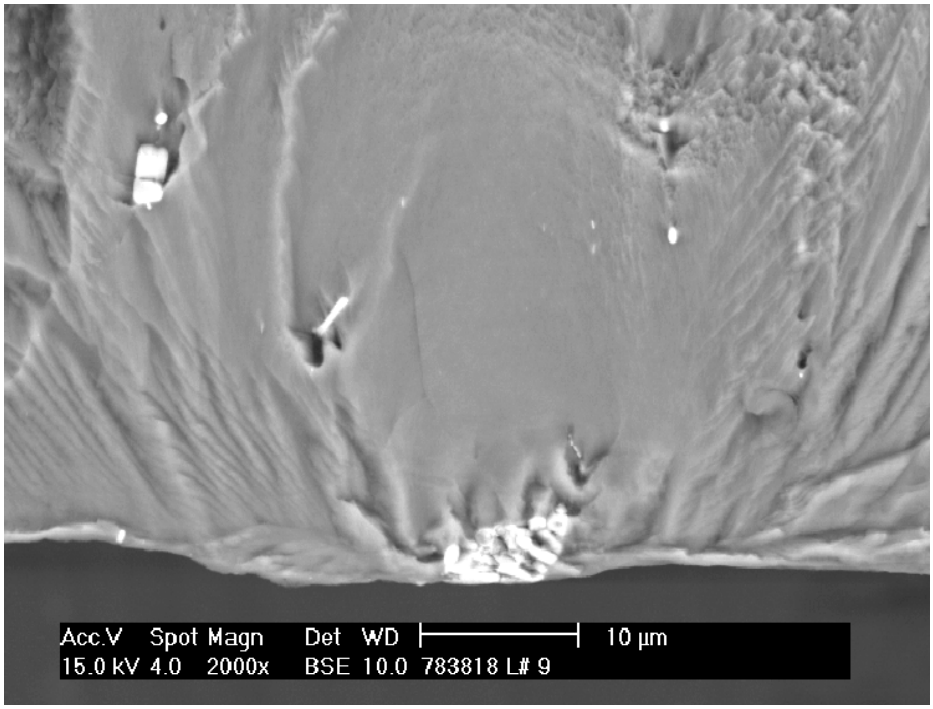

Figure 12 Photomicrograph showing "typical" Al_7Cu_2Fe particle at the initiation site

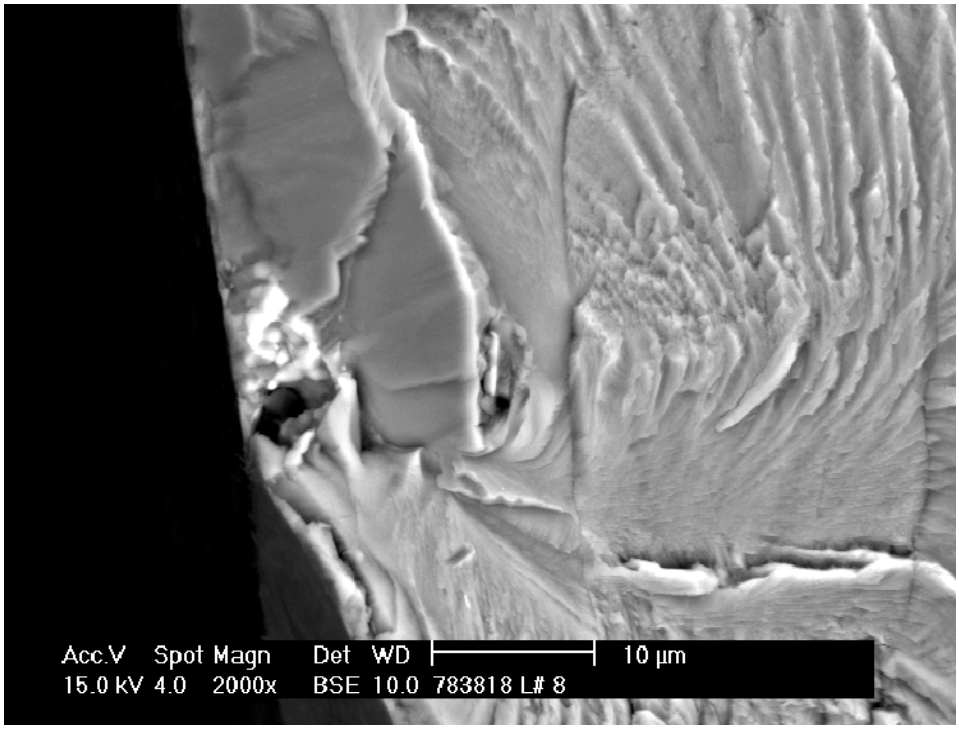

Figure 13 Photomicrograph showing "typical" Al_7Cu_2Fe particle at the initiation site

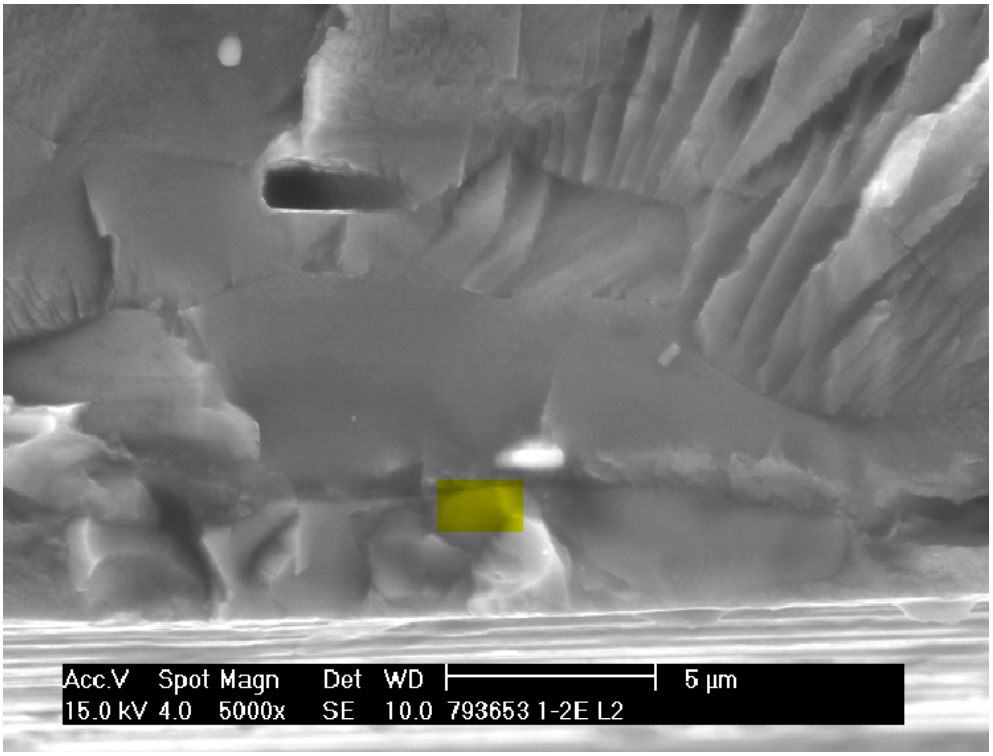

Figure 14 Al_7Cu_2Fe Initiation Site at the surface of the specimen 5000x

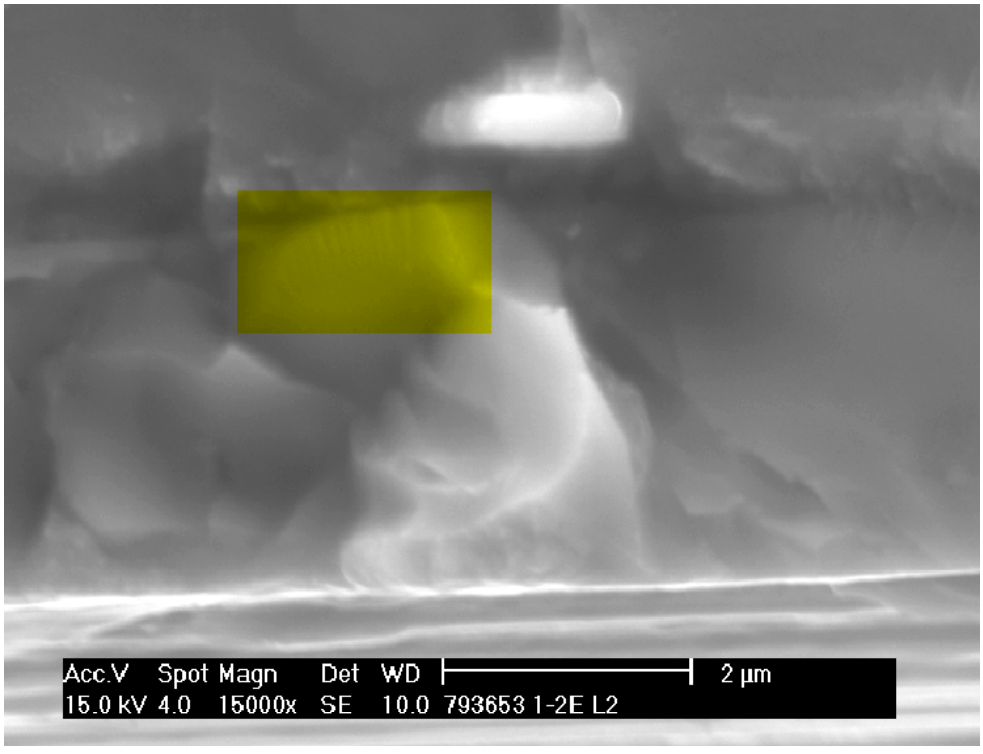

Figure 15 Same Al_7Cu_2Fe particle at 15,000x showing signs of plasticity within the particle

4.5 SEM - Distribution of Fe-bearing and Si-bearing Constituent Particles

The failed round specimens were examined in the SEM to determine the source of the fatigue initiation sites. This analysis revealed that the initiation sites for the edge specimens, which had very high fatigue lives (> 2,000,000 cycles) exhibited stage I initiation, and particle initiation was not present. Stage I initiation is the process whereby concentrated slip forms persistent slip bands (PSB), which will initiate a crack. For the center specimens, which displayed much lower fatigue lives (~100,000 cycles), the initiation site was either an Fe-bearing or Si-bearing constituent particle which was located at or near the surface of the plate.

In order to determine if the Fe-bearing and Si-bearing particle size distribution was appreciably different between the edge and center locations, several maps of large fields of view of sections of the failed round specimens have been acquired by SEM. In theory, it can be envisaged that the amount and/or size of the constituent particles considerably differs between the edge and center locations, which might help to explain why the fatigue lives are different for the various locations.

The results of these maps are shown in Figures 16 and 17. Although the edge locations consistently showed consistently higher number densities of small (less than 10 μm^2) Fe-bearing particles, this was not the case for larger (greater than 10 μm^2) Fe-bearing particles. It is theorized that the larger particles are involved in the fatigue initiation process, and the number density for the larger Si and Fe-bearing particles were fairly constant and at a low level. The Si-bearing particles were at a low number density for all particle sizes. The conclusion that can be drawn is that the particle size distribution does not explain why the edge fatigue lives are longer than the center specimens. More specifically, since the number density of Si-bearing particles is fairly constant for all particle sizes, this alone does not describe why the Si-bearing particles should be more detrimental to fatigue lives than the Fe-bearing particles.

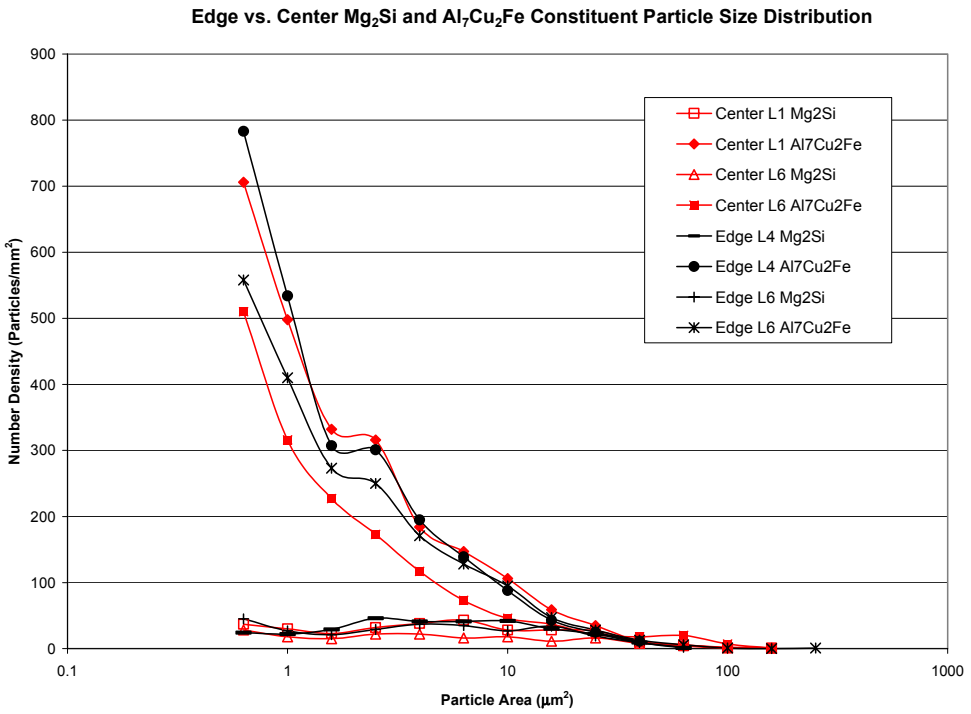

Figure 16 Constituent Particle Distribution Comparing the Edge and Center of the Rolled Plate – All Particles

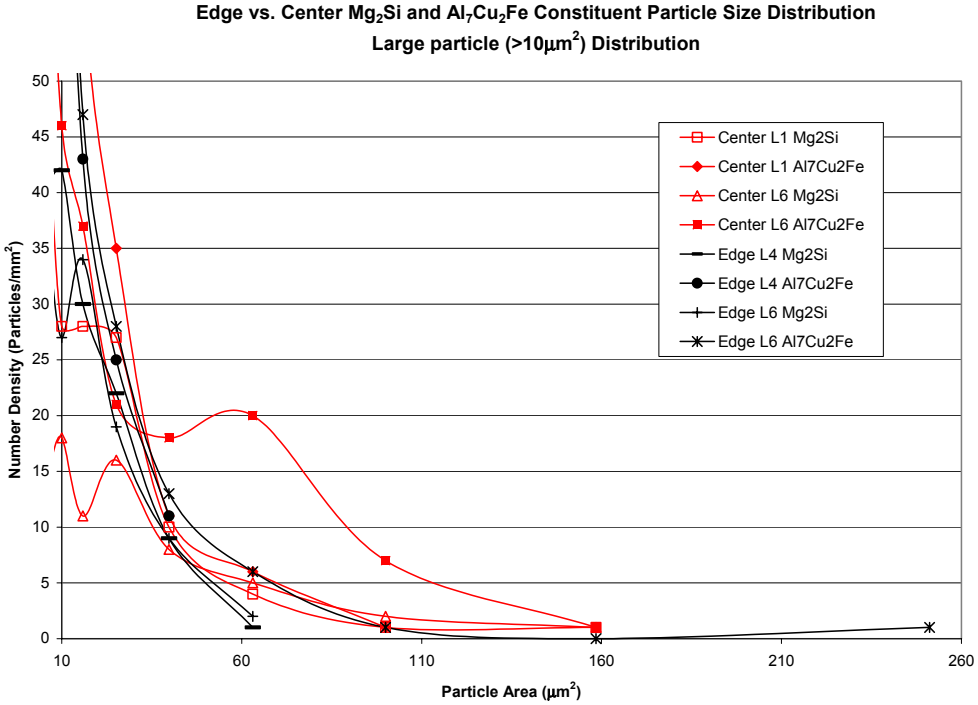

Figure 17 Constituent Particle Distribution Comparing the Edge and Center of the Rolled Plate – Particles Greater Than or Equal to 10 µm^2

Figure 18 displays the area distribution of Fe- and Si-bearing particles as a function of "critical" size, which was selected based on the assumption that there will be some particle size that will become the initiation site for fatigue. The plot does show that the Fe-bearing particles are greater in number density and size for both edge and center locations. Again, since the alloy contains more Fe than Si, this is to be expected; however, it does not explain why the fatigue lives for the edge specimens are longer than those of the center specimens.

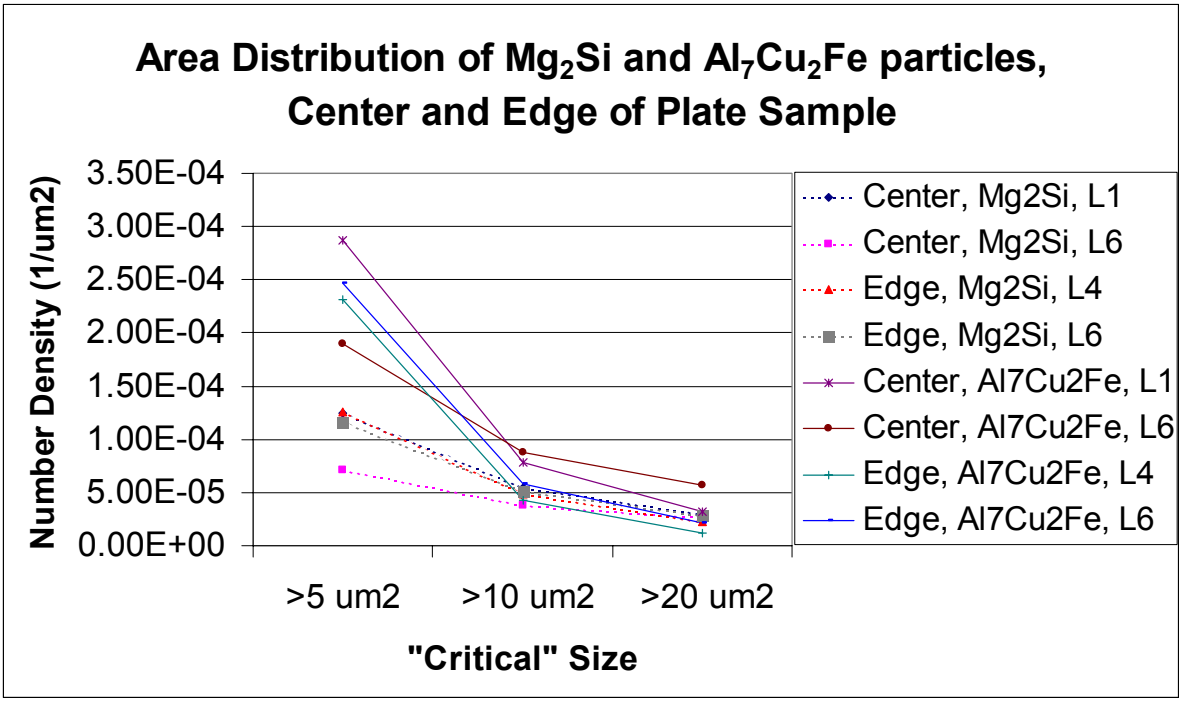

Figure 18 Constituent Particle Density as a Function of Size

4.6 Atomic Force Microscope with Nanoindentation:

The elastic and plastic behavior or properties of the constituent particles themselves may affect the resistance to fatigue initiation. Using an atomic force microscope equipped with a nanoindenter, the elastic and plastic properties of the constituent particles have been examined.

The modulus of an inclusion in a matrix plays an important role in establishing mechanical mismatch and incompatibility stresses at the matrix-inclusion interfaces during mechanical loading. Furthermore, the difference in resistance to plastic deformation between matrix and inclusion must be considered in an attempt to evaluate the role the constituent particles play with respect to fatigue crack initiation. Hence, the mechanical properties of the inclusions and the matrix have been probed locally with an atomic force microscope (AFM), which was equipped with a nanoindenter. The hardness, H, and reduced modulus, E_r, of the Al_7Cu_2Fe and Mg_2Si particles, as well as of the aluminum matrix, have been measured from nanoindentation tests. Since the nanoindentation testing is measuring the plasticity of single crystals, particles or aluminum grains that are oriented differently may result in different hardness values. Hence, any conclusions that are drawn here are specific to the local particles in their unique orientations. Many more nanoindentation tests of the constituent particles and aluminum matrix would have to be performed in order to establish a statistical representation of the entire population of microstructural features. As shown in Table 3, the modulus and hardness for the Fe-bearing particles were determined to be much higher than that of the Si-bearing particles and the matrix.

Table 3 Average and Standard Deviation Values of Contact Depth, Hardness, and Reduced Modulus:

Sample	**hc (nm)**	**Er (Gpa)**	**H (Gpa)**
Bulk Al	123.0 +/- 72.3	75.6 +/- 14.8	2.2 +/- .56
Al_7Cu_2Fe	115.5 +/- 38.7	133.6 +/- 17.8	6.6 +/- 1.4
Mg_2Si	153.2 +/- 89.4	50.1 +/- 5.2	2.5 +/- .94

The nanoindentation tests utilized a 90° cube corner diamond indenter to apply an increasing load in each microstructural feature to achieve a maximum indentation depth of ~300 nm. Once the force-displacement relationship was established (see Figure 19 for

example), the area function ($A(h_c)$) was used to determine the reduced elastic modulus (E_r) and hardness (H) for each indented region [20]:

$$A(h_c) = 2.598h_c^2 + 1.1531e3h_c - 1.5436e4h_c^{1/2} + 2.5091e4h_c^{1/4}$$

The reduced modulus was determined by utilizing the formula: $E_r = S\frac{\sqrt{\pi}}{2\sqrt{A}}$, where S is the unloading stiffness $\left(\frac{dP}{dh}\right)$ and A is the projected contact area. The hardness was determined by formulating the ratio of the maximum load to the contact area: $H = \frac{P_{\max}}{A}$.

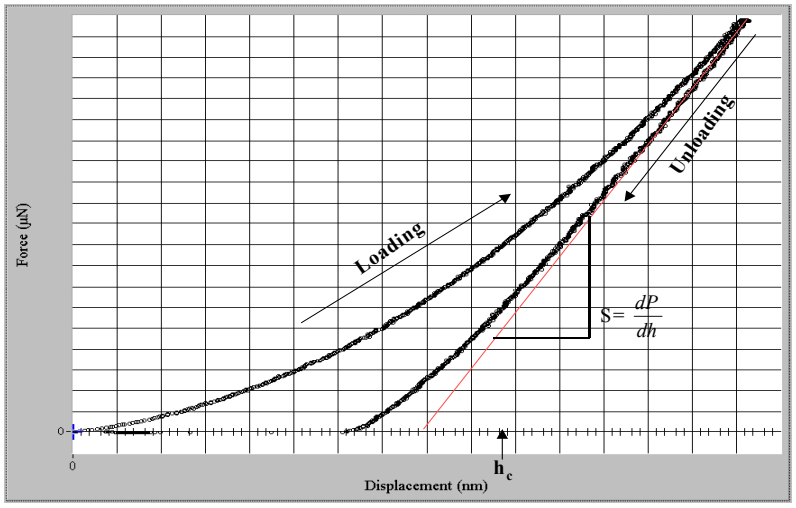

Figure 19 Example of a Load vs. Depth Curve in Fused Quartz

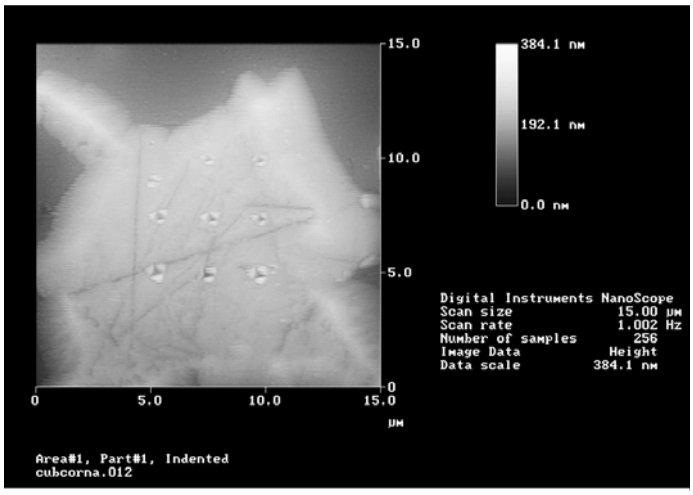

Figure 20 Indented Al_7Cu_2Fe

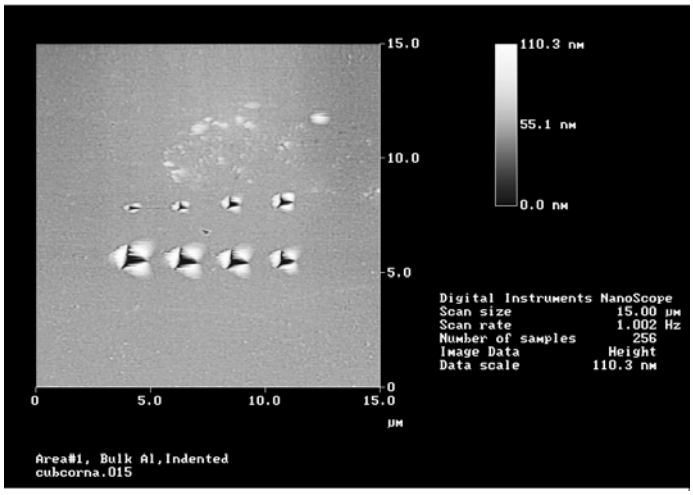

Figure 21 Indented Aluminum Matrix

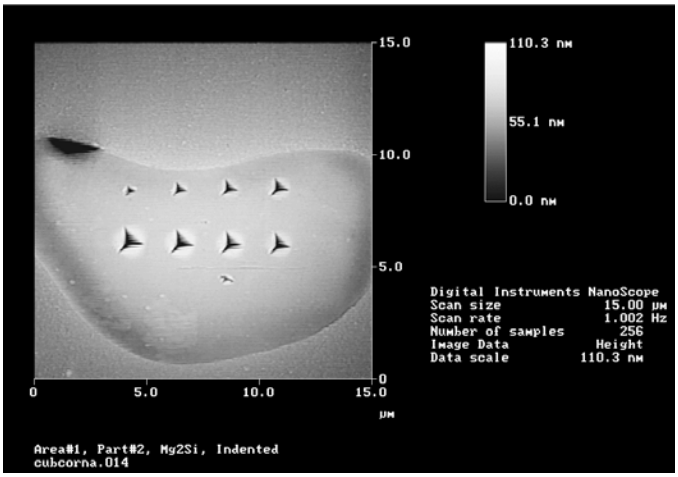

Figure 22 Indented Mg_2Si Particle

The modulus and hardness for the Si-bearing particles were found to be lower than for the alloy matrix and the Fe-bearing particles. It may be inferred that the Mg_2Si will enter the regime of plastic stresses at levels of stress that can be accommodated entirely elastically by the Al-matrix and the Al_7Cu_2Fe particles. The silicide particle cannot withstand a high concentration of dislocations, and can break prior to any other microstructural feature, which will lead to the initiation of a crack. Once the crack is initiated, it can become a preferred site for propagation to occur.

This data is shown schematically in Figure 23, which shows that at a given strain level in the elastic regime, the Fe-bearing particle and the aluminum matrix can withstand a higher level of stress, and still remain in the elastic regime. Another inference that can be made is since the Si-bearing particle and the aluminum matrix have similar yield strengths (analogous with the hardness measurement), the Si-bearing particle will preferentially fracture over the aluminum matrix. This is due to the Si-bearing particle being of finite size as compared to the surrounding bulk aluminum matrix, which can spread the strain over a larger volume. Therefore, the matrix can locally yield, whereas, the Si-bearing particle cannot accommodate the local strains, and is forced to preferentially fracture.

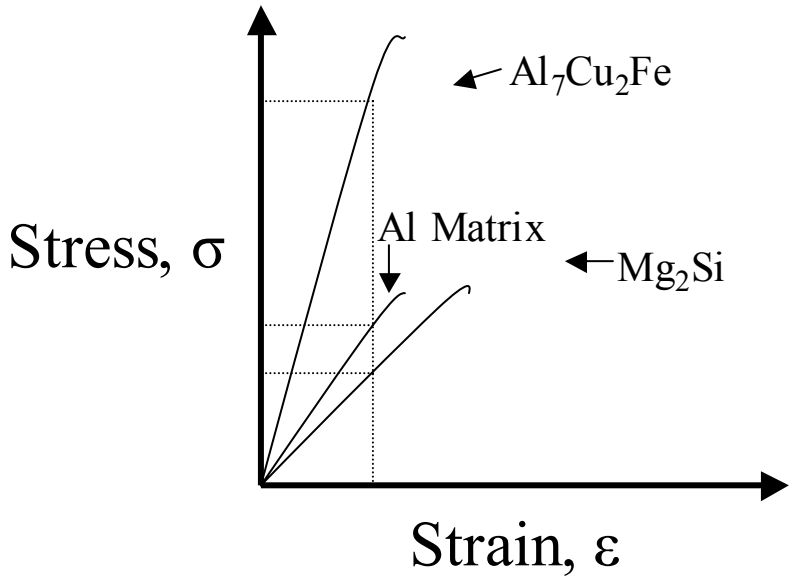

Figure 23 Schematic diagram which displays relative elastic properties of constituent particles and aluminum matrix

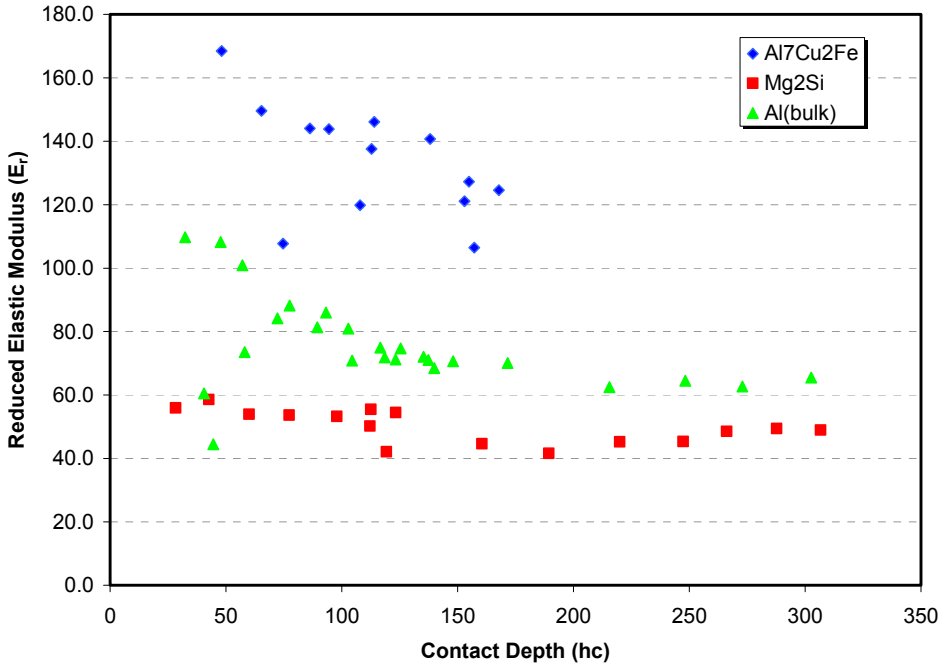

Figure 24 Reduced Elastic Modulus (E_r) vs. Contact Depth (h_c)

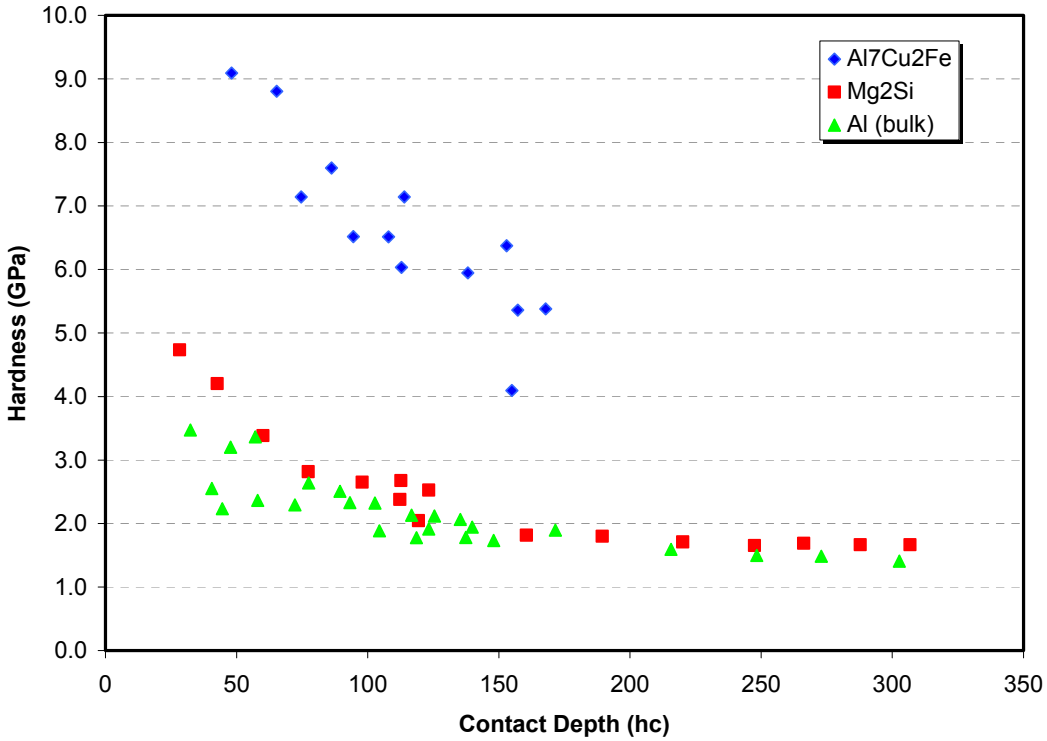

Figure 25 Hardness (H) vs. Contact Depth (h_c)

5.0 GENERAL DISCUSSION

Fatigue initiation in Al-7055-T7751 plate is an important material property, since the application for which it is used, upper wing skin plate in commercial aircraft structures, undergoes high cycle fatigue behavior under everyday use. By studying the hierarchical features that initiate fatigue, one may be able to determine the most important factors that should be considered when trying to improve the fatigue life of this product. Through correlation of microstructure-property relationships, an assessment of the roles of the various hierarchical microstructural features on fatigue life with a focus on initiation has been attempted. Optical light and scanning electron microscopy together with texture measurements by X-ray diffraction, as well as local mechanical testing by nanoindentation with a specialized atomic force microscope, has been completed in an effort to thoroughly characterize the fatigue initiation behavior in this material.

Since the stress-life fatigue behavior of this material displayed a clear improvement in the edge locations as compared to the center locations, a thorough analysis of the width and through-thickness effects was undertaken.

Optical photomicrographs were analyzed comparing the various plate locations. This analysis revealed that although the surface grains were more recrystallized than the mid-plane grains, the edge and center microstructures were very similar at a given thickness location. Therefore, grain structure morphology cannot be responsible for the documented edge-to-center fatigue performance differences.

Pole figure determination and orientation distribution function (ODF) were employed to determine if preferred grain orientation might be playing a role in the fatigue performance differences. Again, although through-thickness texture differences were noted, the edge and center locations exhibited similar textures for a given thickness location. A shear texture existed near the surface, whereas a plane strain or hot rolling type texture was present near the mid-thickness. For a hot rolled 7xxx alloy plate material this is the expected texture. Therefore, the level and type of preferred orientation cannot explain the edge-to-center fatigue performance differences.

By using a field emission gun scanning electron microscope (FEG SEM), and utilizing imaging techniques and energy dispersive x-ray spectroscopy (EDS) analysis,

several fatigue crack initiation sites were analyzed. This analysis revealed that the crack initiation sites associated with Mg_2Si constituent particles exhibited shorter fatigue lives than samples with initiation sites associated with Al_7Cu_2Fe constituent particles. Additionally, the Si-containing particles appeared brittle in nature, since the fractured surfaces were always cleaved. However the Fe-bearing particles, in many cases, displayed more ductility, since some of the particles showed signs of plasticity within the particles themselves.

Depending upon the orientation of the constituent particles within the matrix the number of active slip systems could have an effect on the pile-up of dislocations against the particle. If several slip systems are active, the dislocations could be less damaging to the particle, since they will not produce such an intense pile-up stress as a planar or persistent slip band of dislocations. The matrix could activate the glide of dislocations to another active slip system and dissipate some or all of the pile-up stress. If, however, there is a low number of active slip systems, the pile-up stress will continue to rise to a level sufficient to produce a crack, presumably across the constituent particle, and hence, the crack could begin to propagate. This condition of having limited available slip systems could potentially lend itself to rationalize lower fatigue lives.

Several maps of large fields of view of the failed round specimens were acquired by SEM. From these maps, the size distribution, area fraction, and spatial distributions of Fe-bearing and Si-bearing particles were obtained. The initial analysis of particle size alone did not fully describe why the Si-bearing particles were more damaging than the Fe-bearing particles. However, the area and spatial distributions may shed more light onto why the fatigue lives for the edge specimens are typically longer than those for the center specimens. As shown in Figure 16, the edge and center specimens both have consistently larger number densities of Al_7Cu_2Fe particles than Mg_2Si particles that have particle areas less than 10 μm^2. Interestingly, Figure 17 shows that for the distribution of larger particles (>10 μm^2), there appears to be a "critical" area/size of ~60 μm^2, at which the majority of particles above this size are center specimens. One could potentially infer from observation the argument that the larger particles located in the center specimens are more detrimental from a fatigue standpoint than the numerous Fe-bearing constituent particles that are more equally distributed in both the center and edge specimens. Further studies should be conducted to confirm such a hypothesis.

Using an atomic force microscope (AFM) equipped with a nanoindenter, the elastic and plastic properties of the constituent particles have been examined. The modulus and hardness values for the Si-bearing particles were found to be lower than the aluminum matrix and the Fe-bearing particles. One may infer from this information that the Si-bearing particle may thus enter the regime of plastic stresses at local strains far below those that could be accommodated elastically by the Fe-bearing particles and the matrix. Conversely, at a suitable given level of local stress, that can be accommodated elastically in the stiffer Al_7Cu_2Fe and Al-matrix, the Mg_2Si would already have to deform plastically or even fracture. Since this testing is performed on single crystals, particles that are oriented differently could yield results that differ from those presented here. Hence, the statistical relevance and validity of these few experimental measurements and AFM observations may be questionable. However, the observations represent an interesting result that confers with the fatigue data.

Thus, in conclusion, the experimental work clearly indicates that grain morphology and texture can, with reasonable certainty, be ruled out as possible reasons for the documented fatigue life performance difference between edge and center locations. Further, it appears likely that the spatial distribution of the larger constituent particle present in the populations of constituent particles is associated with the observed fatigue life performance differences.

6.0 SUMMARY AND OUTLOOK

By utilizing various analytical techniques, an assessment of the roles of various hierarchical microstructural features on fatigue life has been attempted. The fatigue lifetimes of the specimens extracted from the edge of the plate exhibited higher lifetimes than the specimens extracted from the center location. Upon comparing the initiation sites of the fatigue specimens in the scanning electron microscope, lower lifetimes were typically associated with Mg_2Si particles, whereas, higher lifetimes typically contained Al_7Cu_2Fe particles. In viewing the microstructures in the optical microscope, the various width and thickness locations were similar.

From a statistical standpoint, the edge location exhibited a much higher probability of having a longer fatigue life than the center location, particularly at low stress levels. In comparing the size and distribution of the Fe and Si-bearing particles by location, the center location did display a higher number density of larger Fe-bearing particles (> 10 μm^2) than Si-bearing particles; however, the number density of Si-bearing particles was fairly constant for both edge and center locations, regardless of particle size. It is interesting to note that the number density of smaller (~5 μm^2) Fe-bearing particles was higher than the Si-bearing particles for both locations, but these smaller particles typically are not involved in the initiation process.

By utilizing an atomic force microscope equipped with a nanoindenter, the elastic and plastic properties of the Mg_2Si and Al_7Cu_2Fe particles were measured and compared with the aluminum matrix. This analysis revealed that the Si-bearing particles are very similar to the aluminum matrix; whereas, the Fe-bearing particles have a higher modulus and hardness than both the matrix and the Si-bearing particles. This may account for the higher fatigue lives associated with the Fe-bearing initiation sites, since the Fe-bearing particles can accommodate higher strain localization prior to particle cracking. In addition, the Fe-bearing particles displayed some plasticity; whereas the Si-bearing particles displayed a brittle behavior, and appeared cleaved in all cases examined.

Texture measurements revealed that the edge and center locations had very similar orientations; whereas, through-thickness measurements showed a shear texture exists near

the surface, while a plane strain texture exists near the mid-thickness, gradually increasing further through the depth.

Thus, there are several main conclusions that can be drawn, based on the data that has been presented:

- If the size and/or spatial distribution of the constituent particles could be "engineered" to favorable levels fatigue life could be enhanced at higher levels of Fe and Si
    - Ideally, eliminate critical-sized constituent particles
    - Smaller, more round and uniformly spaced particles would promote homogenous slip, and improve fatigue performance
- Statistical analysis revealed improved fatigue crack initiation resistance near the edge location over the center location
- Fraction recrystallized, microstructural morphology and texture showed no effect on fatigue crack initiation resistance
- Si is more detrimental to fatigue crack initiation resistance than Fe
- Size distribution of Al_7Cu_2Fe and Mg_2Si may play a role in the fatigue crack initiation resistance
- AFM/nanoindentation revealed that the Al_7Cu_2Fe particles may be more resistant to fatigue crack initiation than Mg_2Si particles

Future studies could be performed to study the relationship and potential manipulation of the orientation and distribution of Mg_2Si and Al_7Cu_2Fe particles with the surrounding matrix. There appears to be a size and morphology effect of the constituent particles that, if properly designed, could have a positive impact on the fatigue life of this product.

APPENDIX A

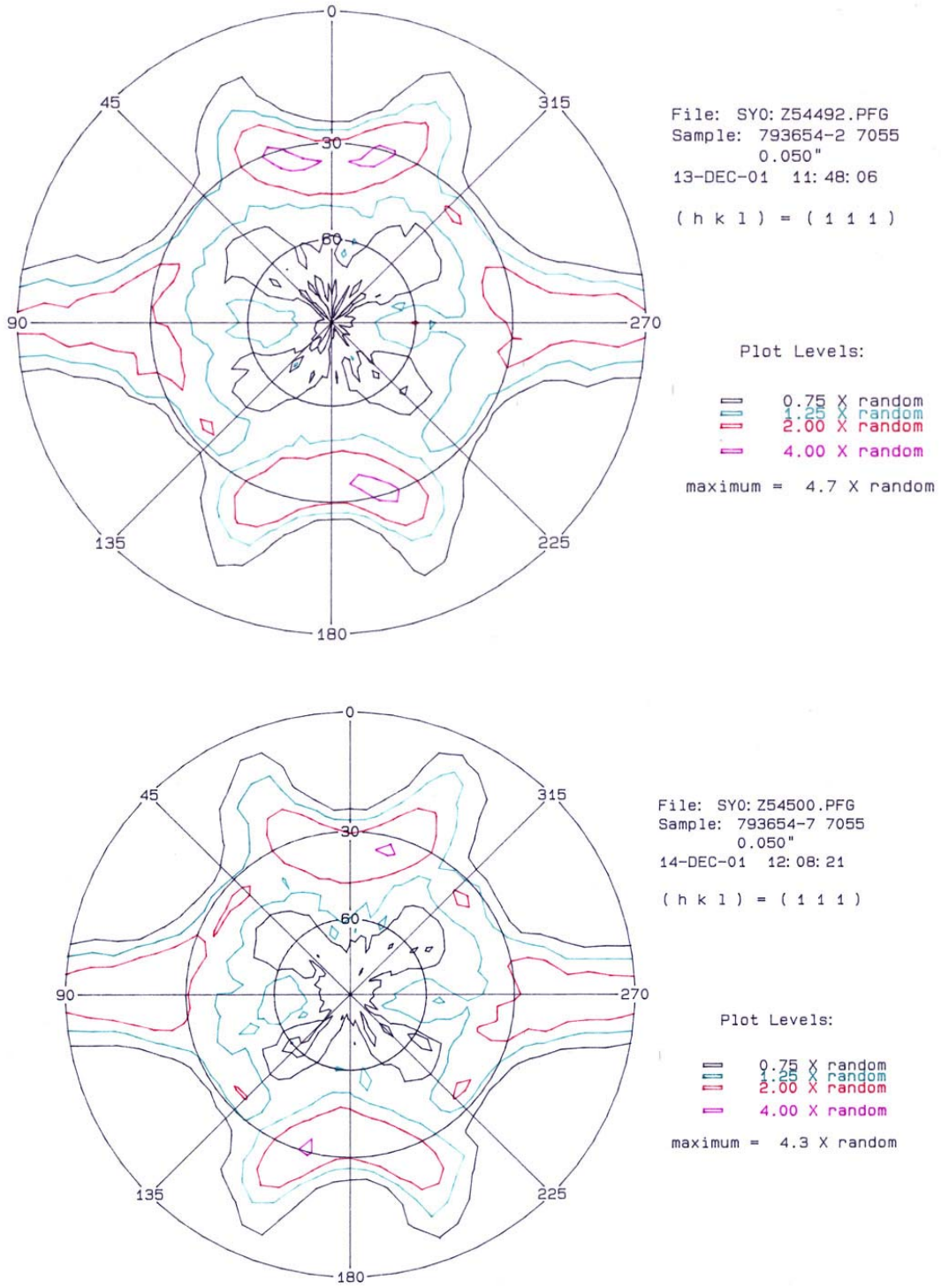

Figure 26 Pole Figures (hkl=111) of 7055-T7751, 0.97 inch Plate. Specimen was machined 0.050 inch from top surface. Top: 4 inches from edge of plate / Bottom: Mid width of 90 inch wide plate

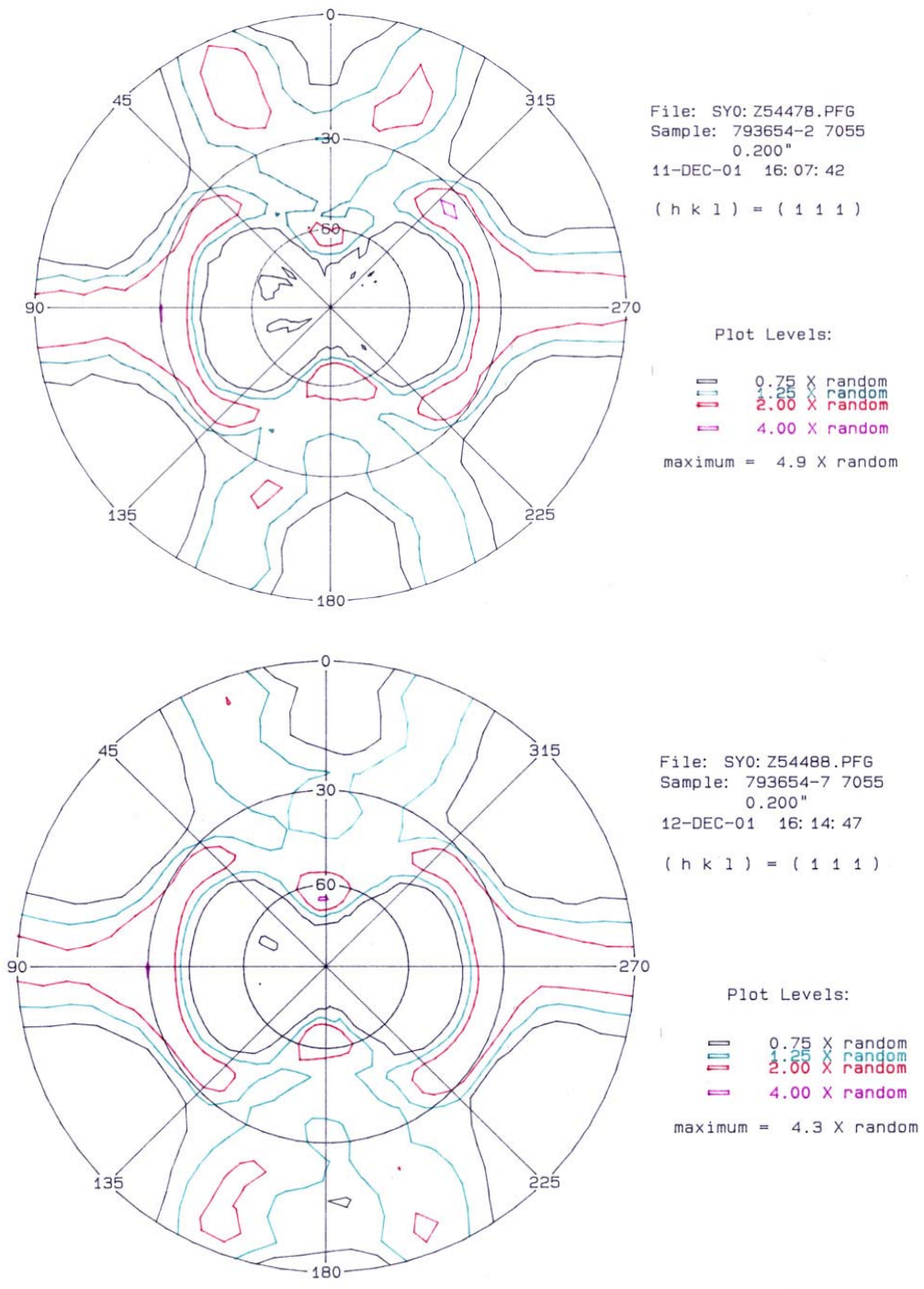

Figure 27 Pole Figures (hkl=111) of 7055-T7751, 0.97 inch Plate. Specimen was machined 0.200 inch from top surface. Top: 4 inches from edge of plate / Bottom: Mid width of 90 inch wide plate

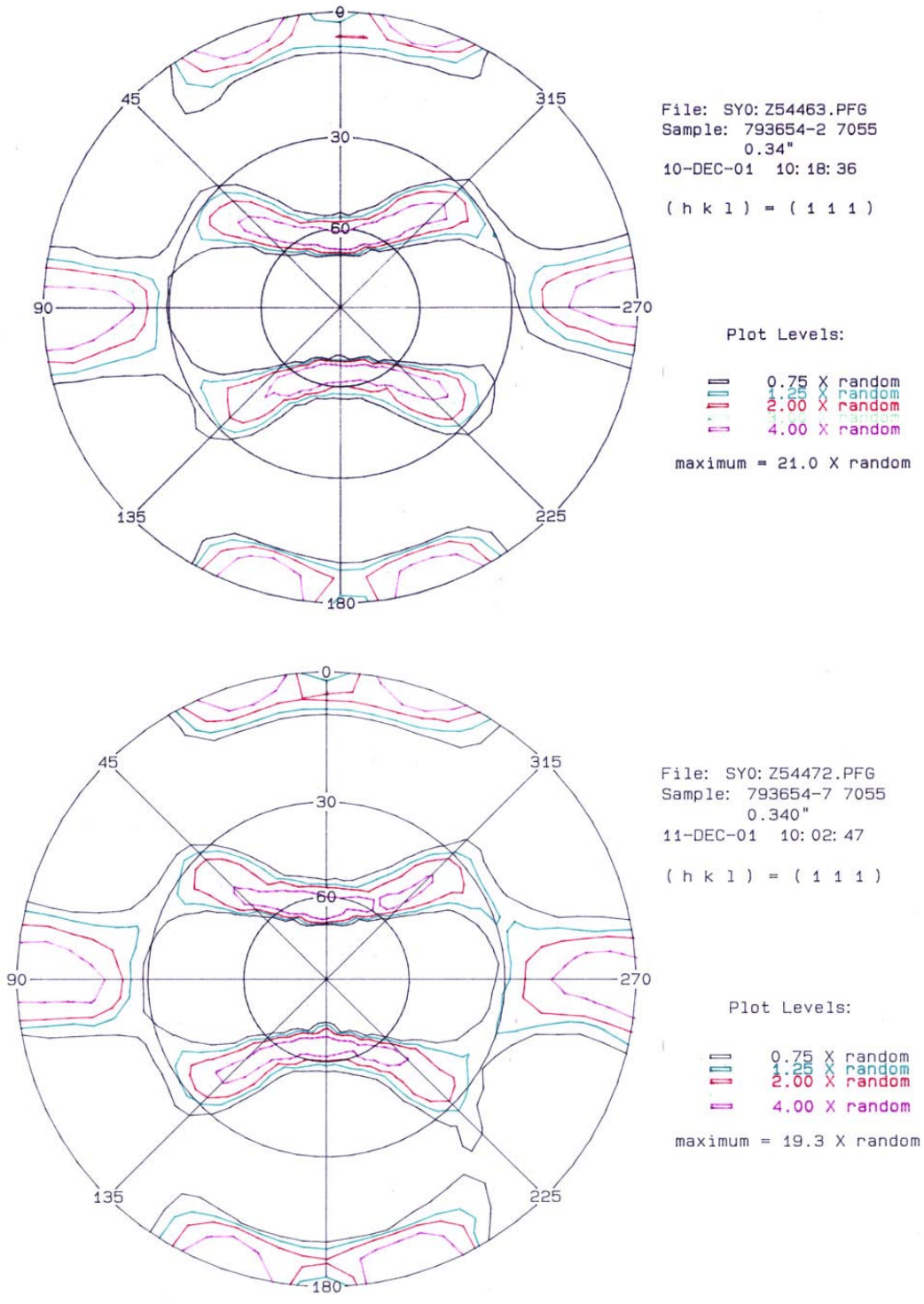

Figure 28 Pole Figures (hkl=111) of 7055-T7751, 0.97 inch Plate. Specimen was machined 0.340 inch from top surface. Top: 4 inches from edge of plate / Bottom: Mid width of 90 inch wide plate

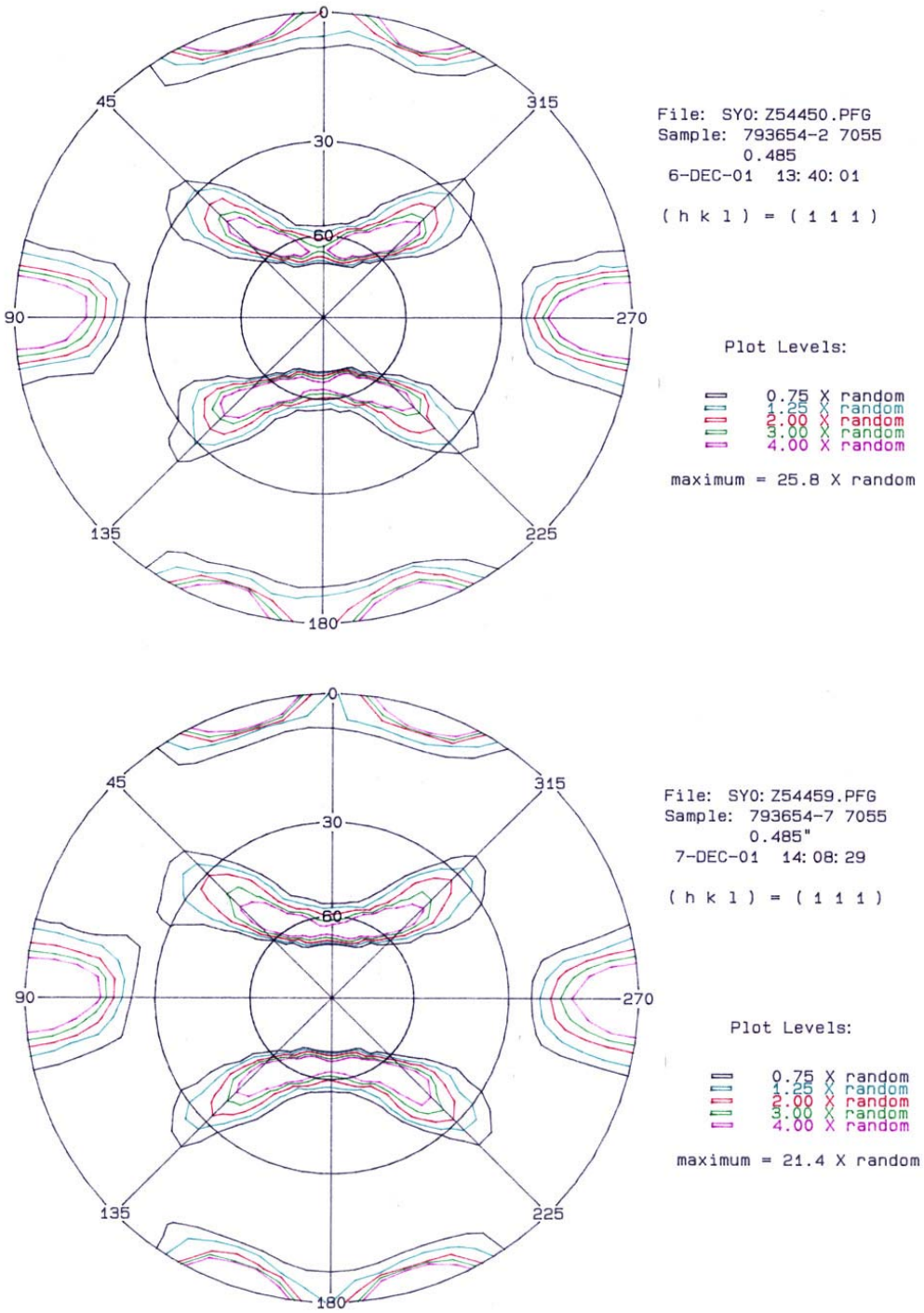

Figure 29 Pole Figures (hkl=111) of 7055-T7751, 0.97 inch Plate. Specimen was machined 0.485 inch from top surface. Top: 4 inches from edge of plate / Bottom: Mid width of 90 inch wide plate

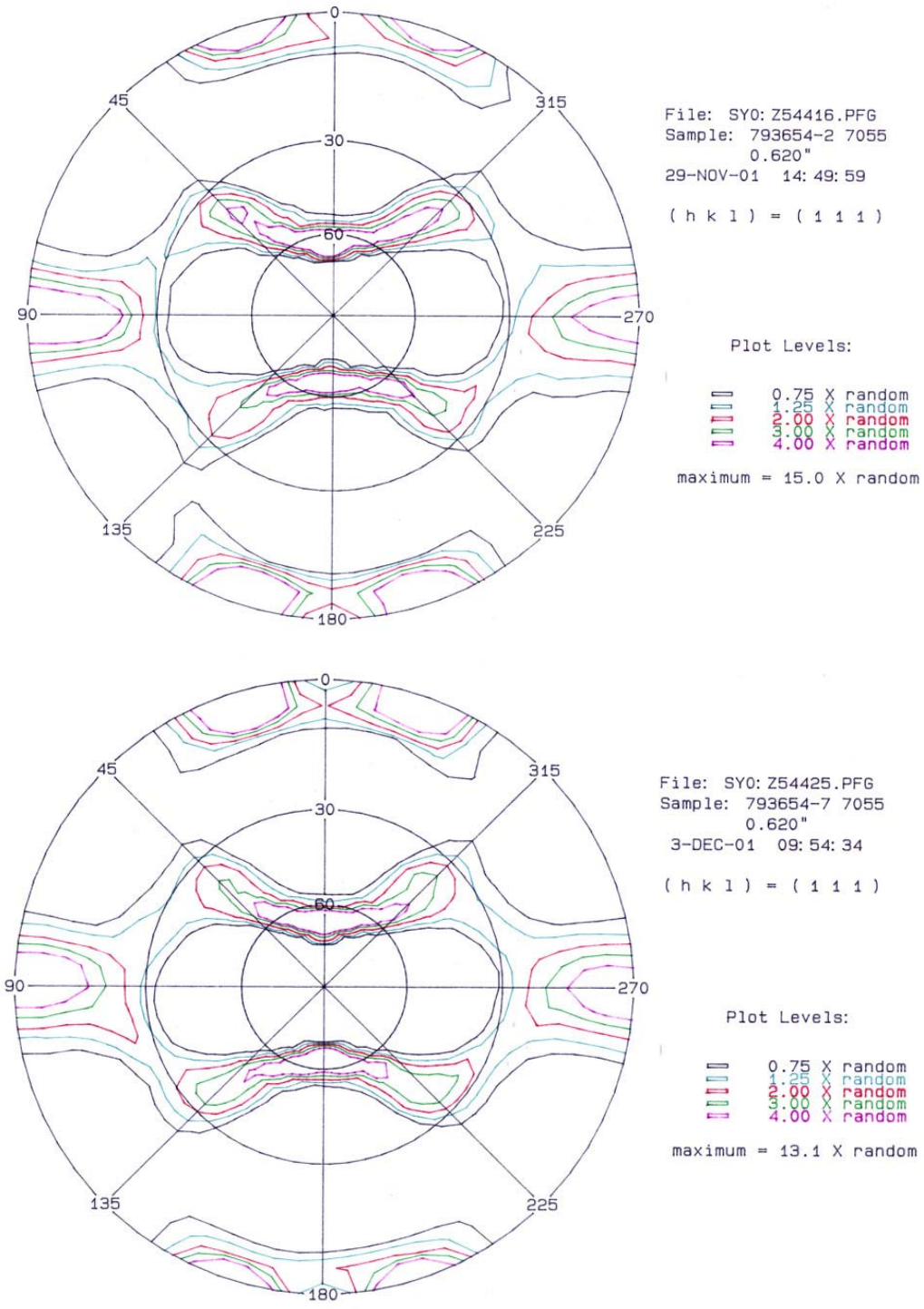

Figure 30 Pole Figures (hkl=111) of 7055-T7751, 0.97 inch Plate. Specimen was machined 0.620 inch from top surface. Top: 4 inches from edge of plate / Bottom: Mid width of 90 inch wide plate

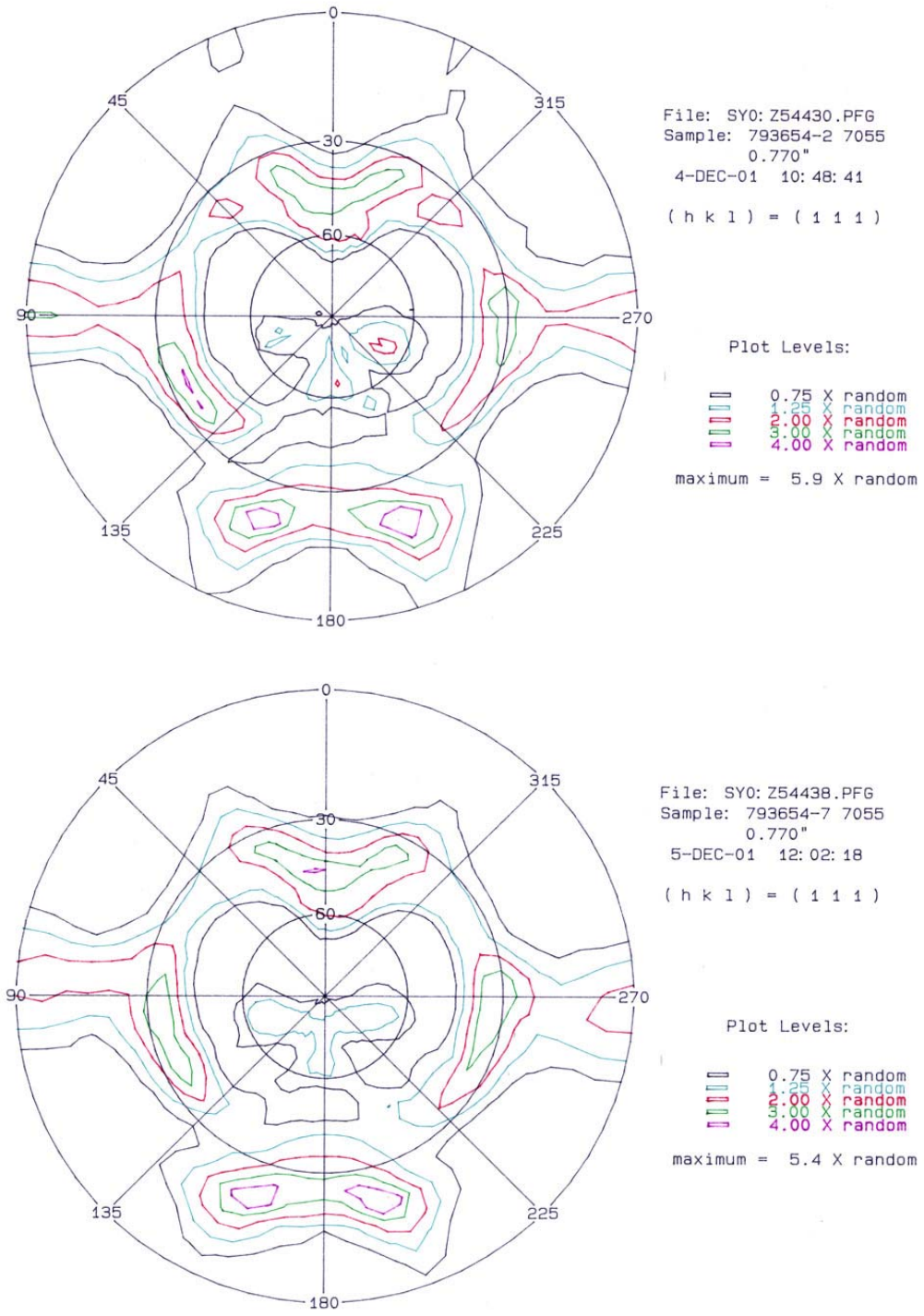

Figure 31 Pole Figures (hkl=111) of 7055-T7751, 0.97 inch Plate. Specimen was machined 0.770 inch from top surface. Top: 4 inches from edge of plate / Bottom: Mid width of 90 inch wide plate

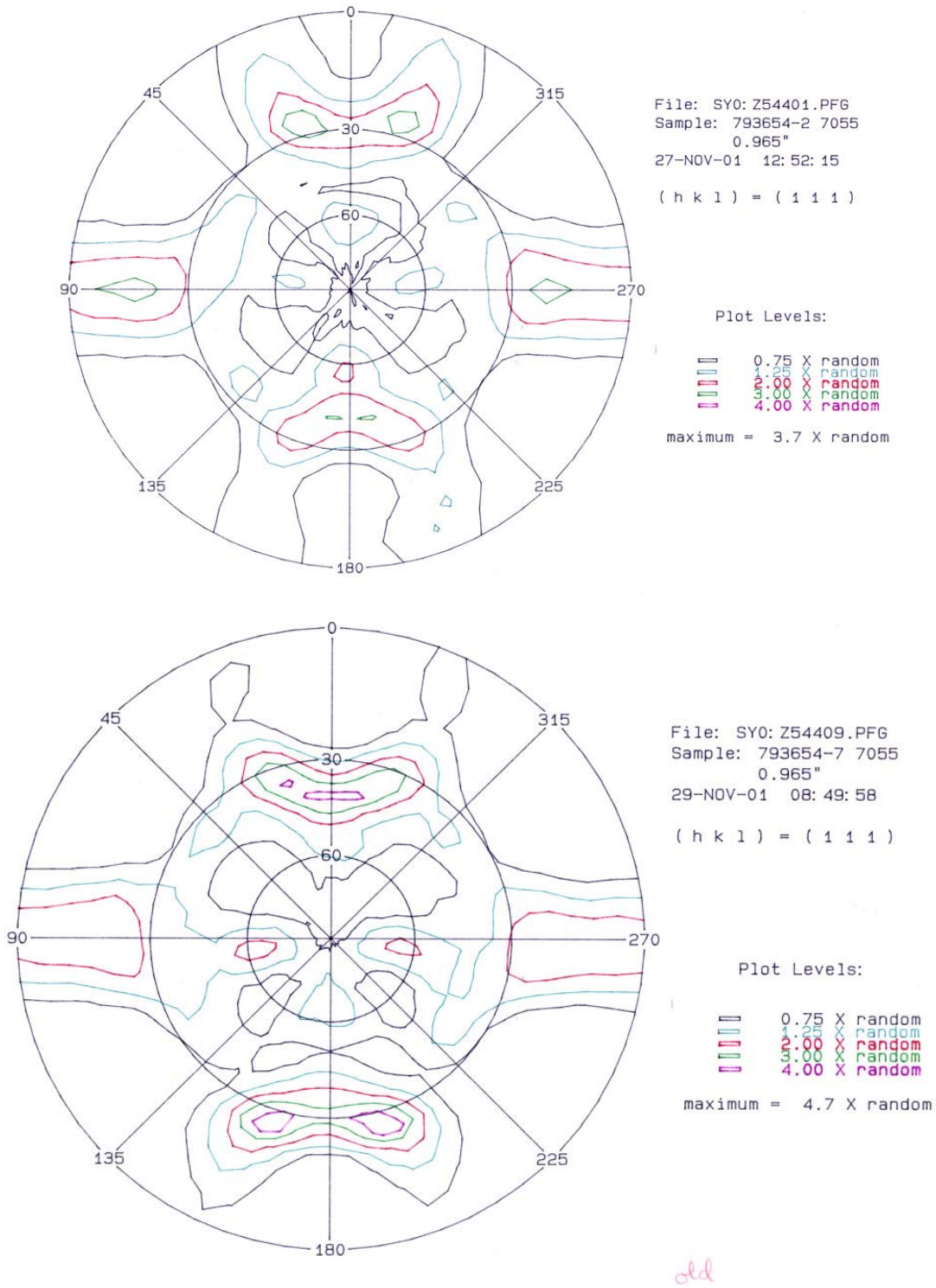

Figure 32 Pole Figures (hkl=111) of 7055-T7751, 0.97 inch Plate. Specimen was machined 0.965 inch from top surface. Top: 4 inches from edge of plate / Bottom: Mid width of 90 inch wide plate.

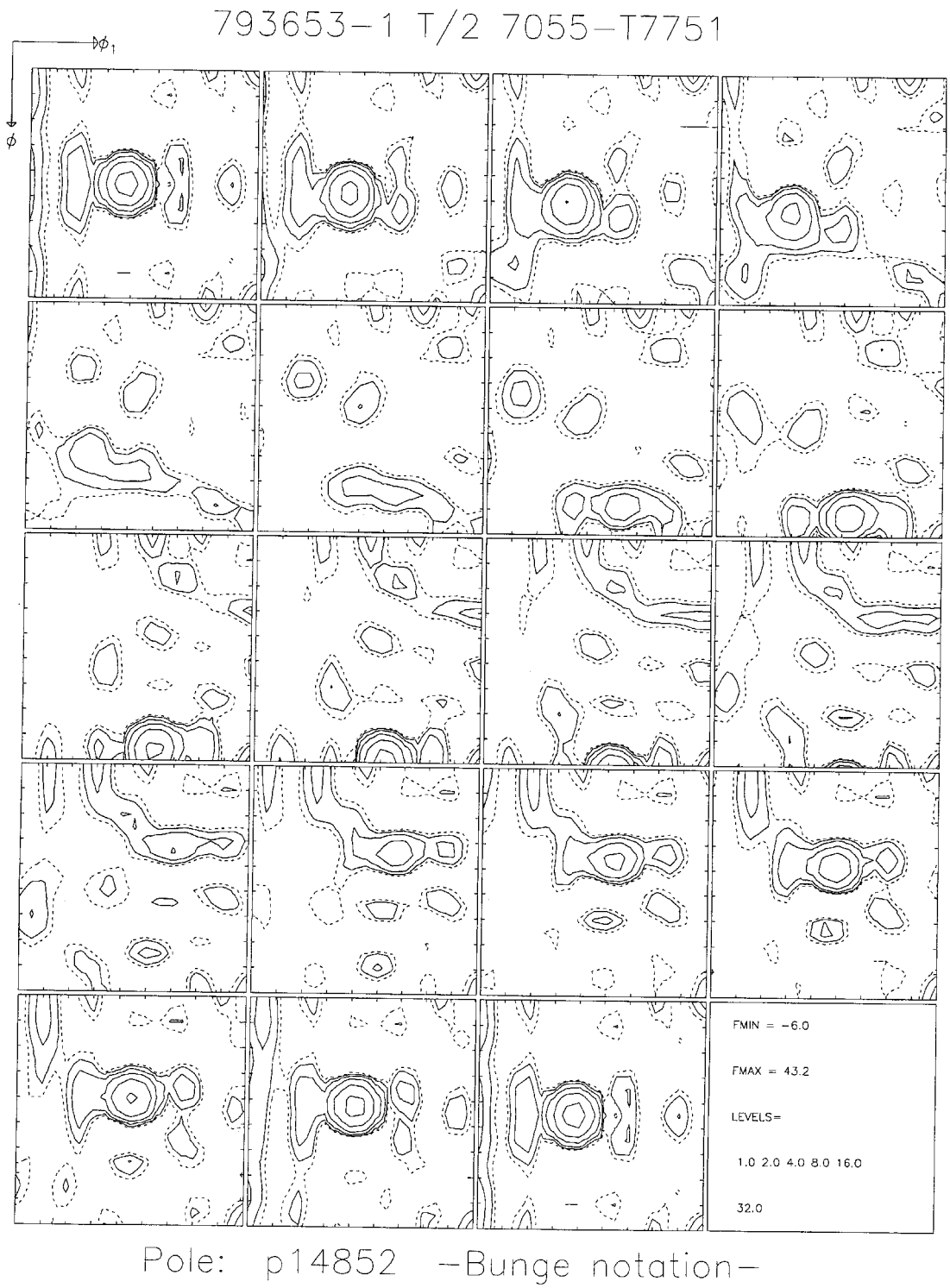

Figure 33 Orientation Distribution Function for t/2 Location, Plate Edge (113,972 Cycles)

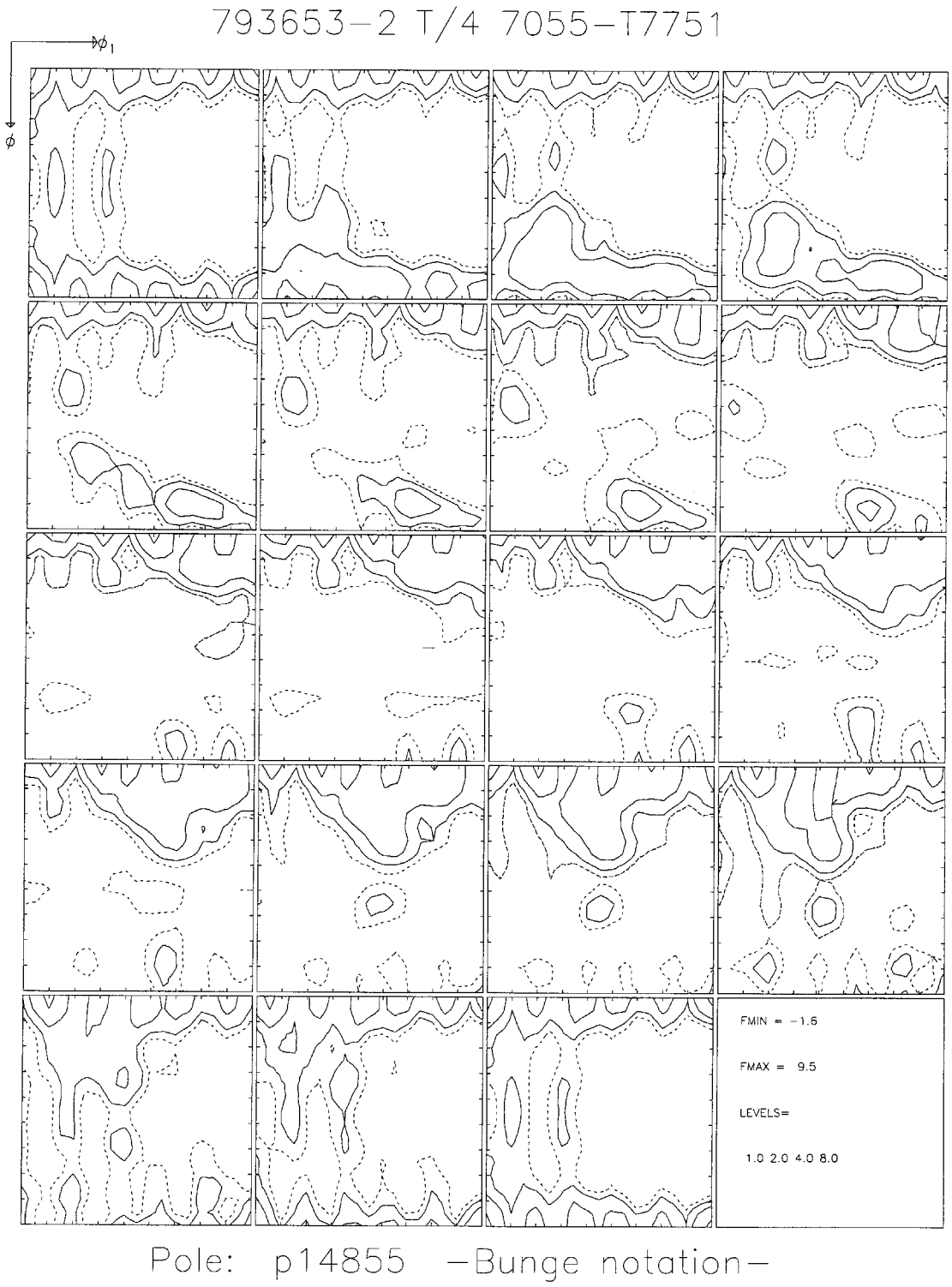

Figure 34 Orientation Distribution Function for t/4 Location, Plate Edge (75,268 Cycles)

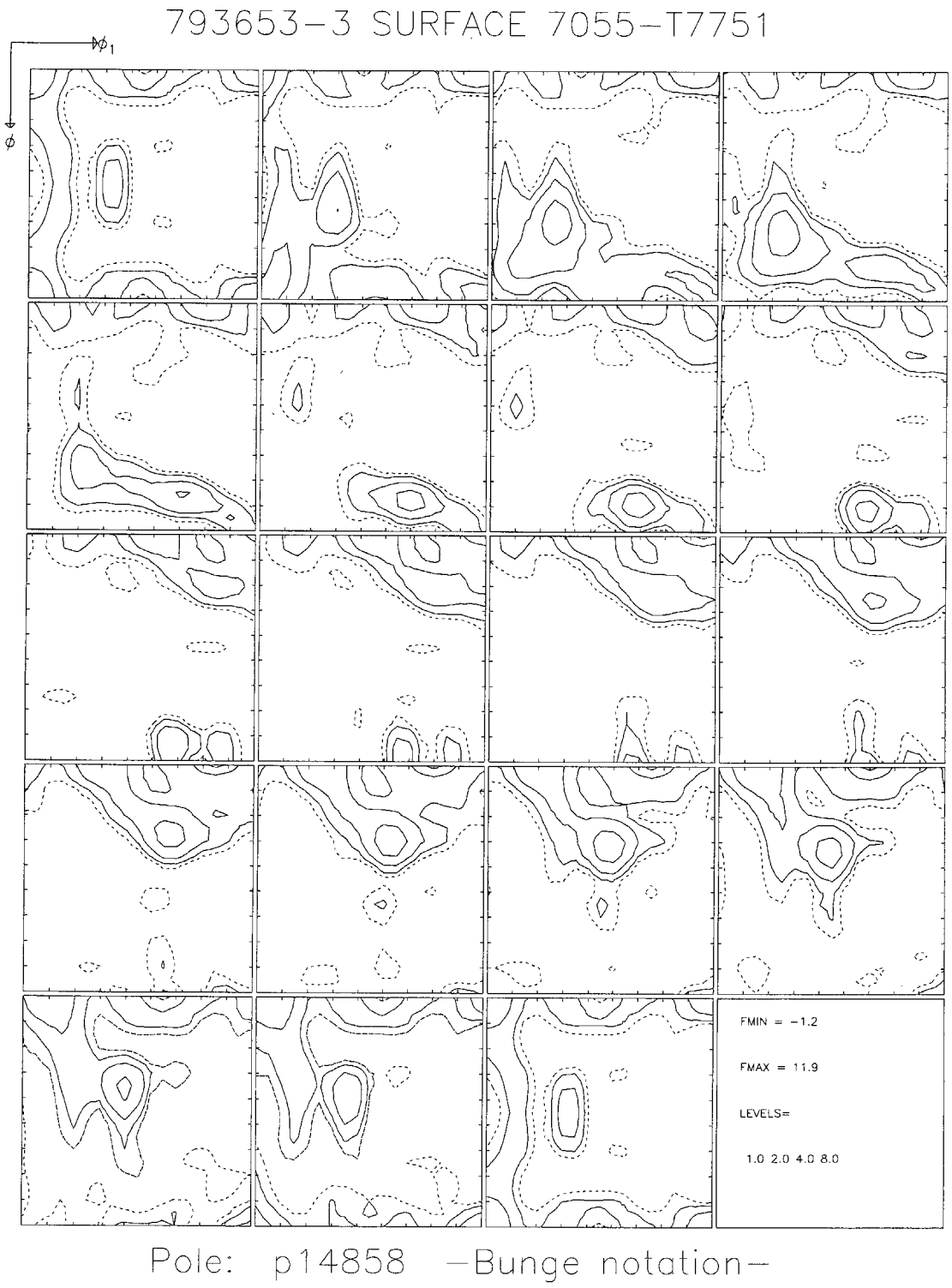

Figure 35 Orientation Distribution Function for Surface Location, Plate Edge (228,628 Cycles).

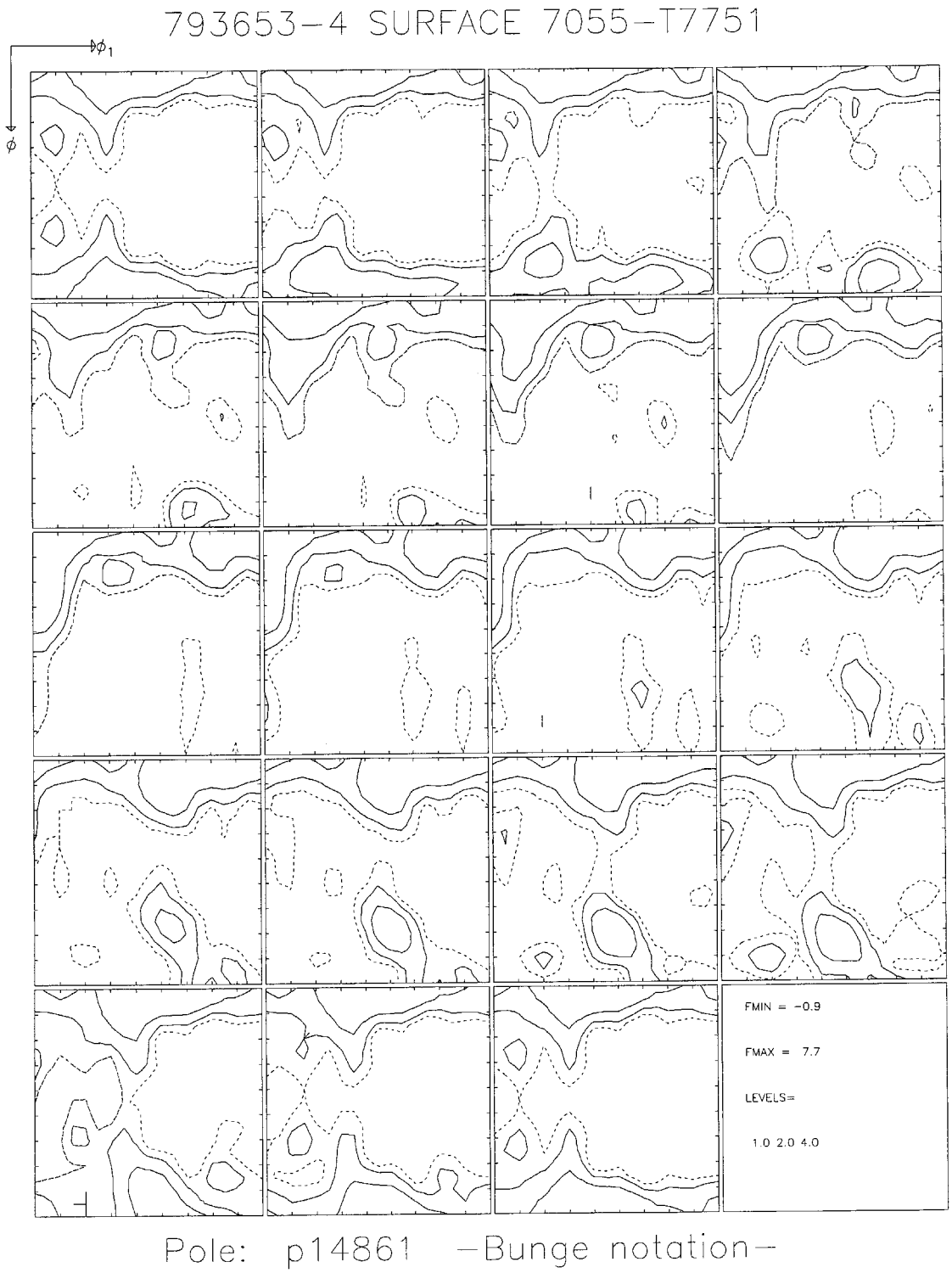

Figure 36 Orientation Distribution Function for Surface Location, Plate Edge (62,150 Cycles)

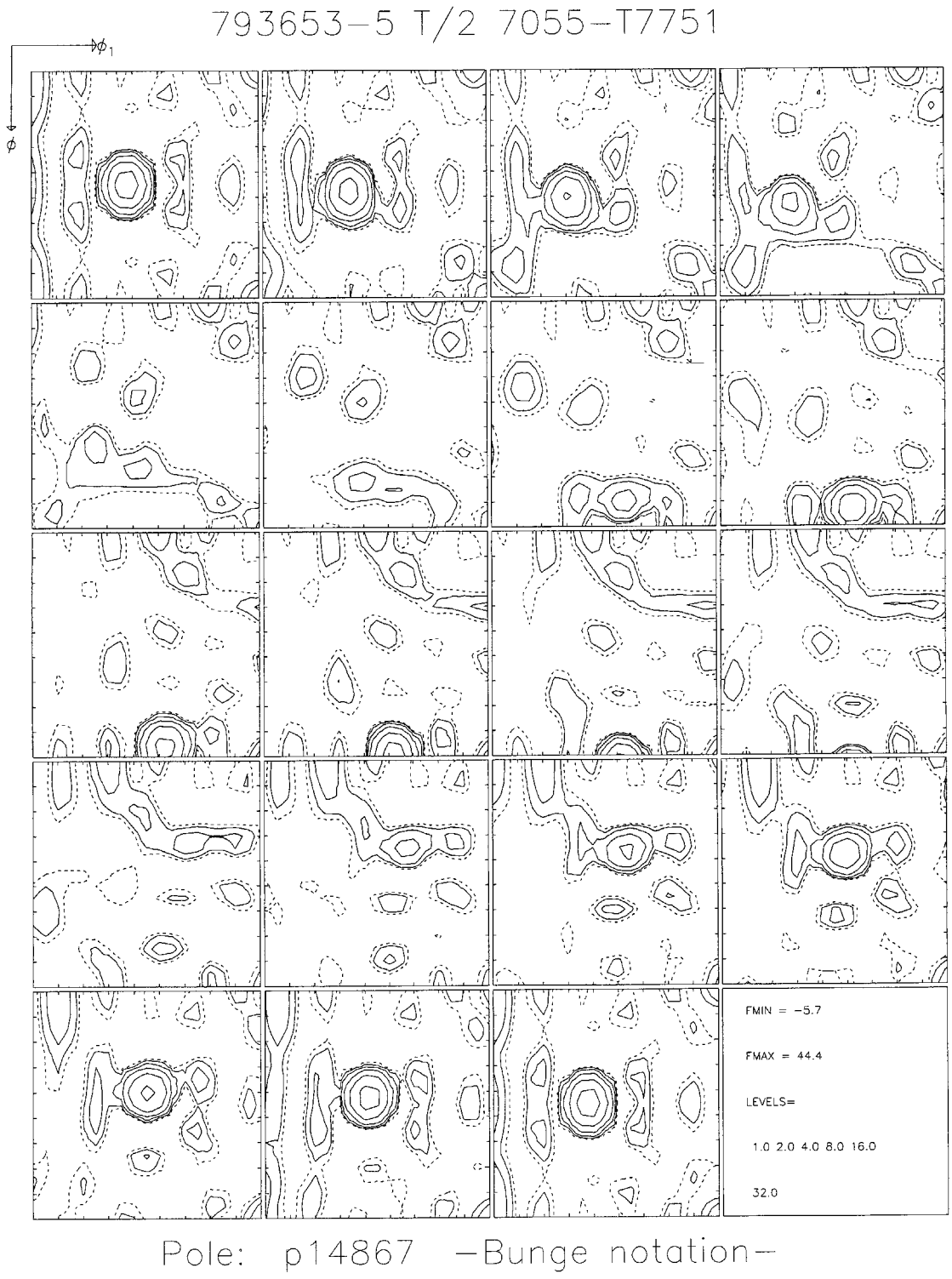

Figure 37 Orientation Distribution Function for t/2 Location, Plate Center (99,463 Cycles)

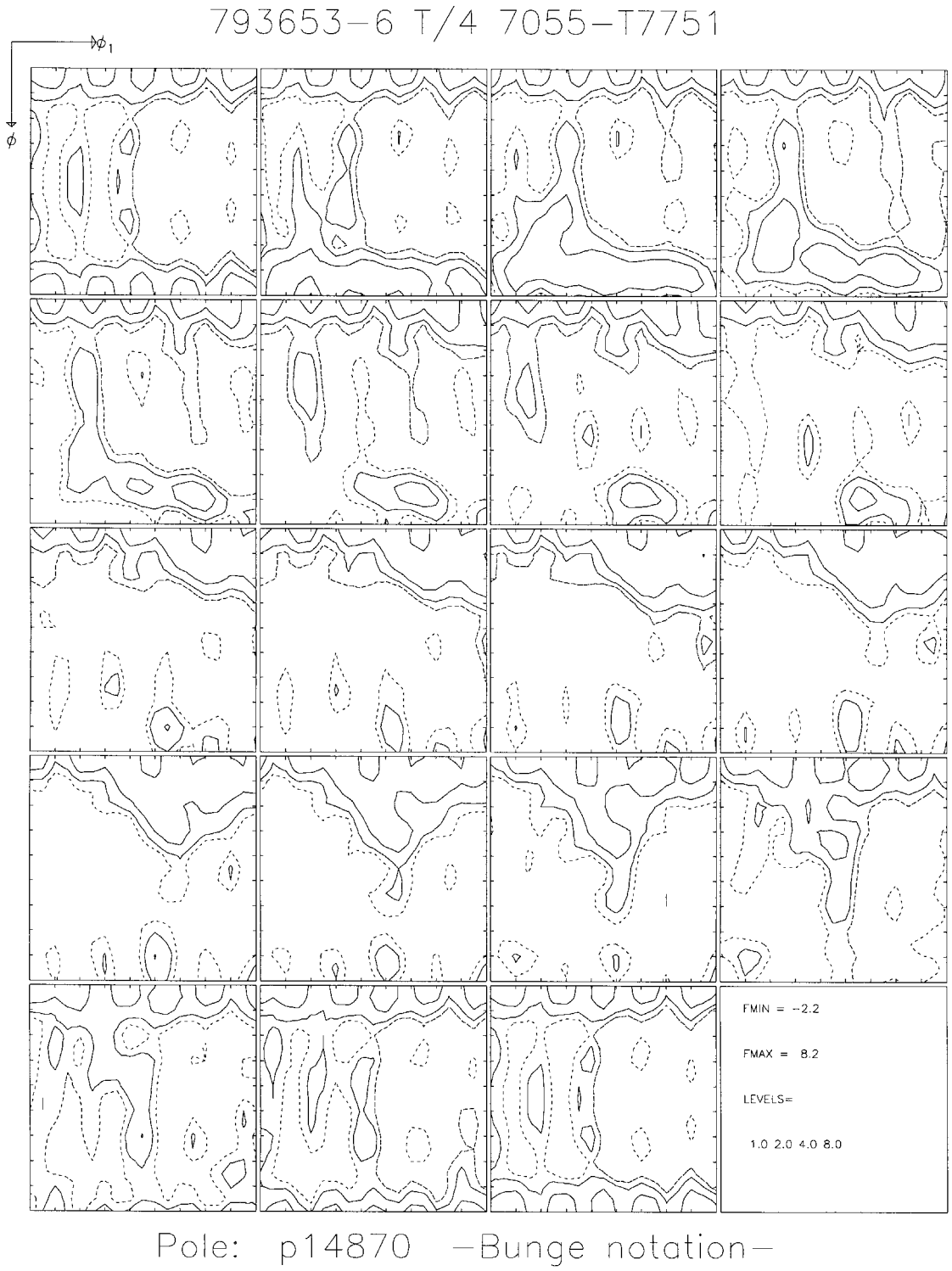

Figure 38 Orientation Distribution Function for t/2 Location, Plate Center (68,977 Cycles)

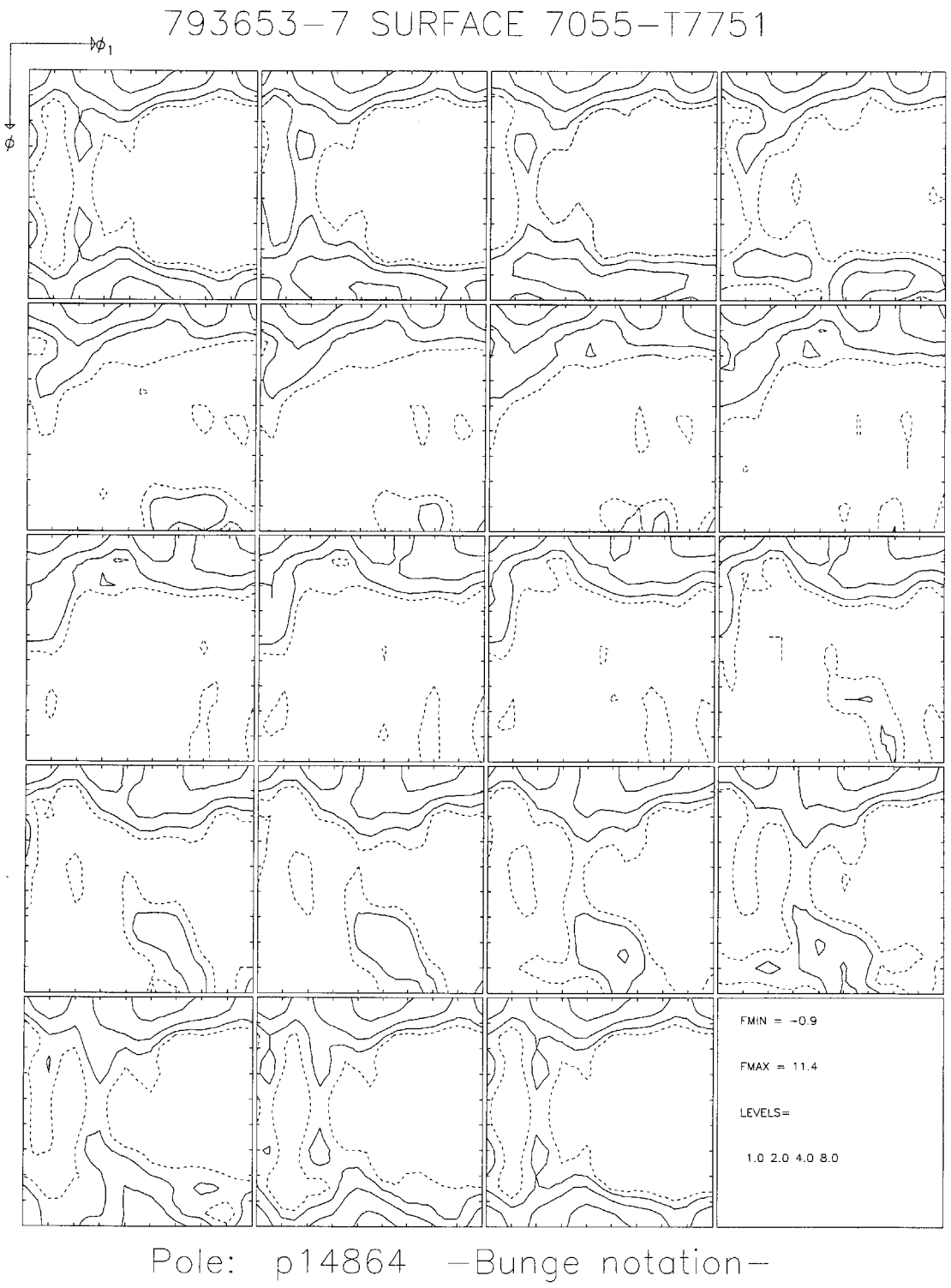

Figure 39 Orientation Distribution Function for Surface Location, Plate Center (55,694 Cycles)

BIBLIOGRAPHY

1. Brockenbrough, J.R., Hinkle, A.J., Magnusen, P.E., Bucci, R.J., "Microstructurally Based Model of Fatigue Initiation and Growth," ONR Contract N00014-91-C-0128, 1994 April 7.

2. Schijve, Jaap, Fatigue of Structures and Materials, Kluwer Academic Publishers, 2001, p.

3. Cooper, Thomas D. and Kelto, Clifford A., Fatigue in Machines and Structures, in Fatigue and Microstructure, Metals Park: ASM (1978) 29-56.

4. Tiffany, C.F., "The Role of Inspections in the Maintenance of Aircraft Safety," presented at the Government/Industry Workshop on NDI Reliability, Houston, Texas, 2-4 September 1978.

5. Magnusen, P.E., "Fatigue failure analysis from 7050 plate summer ingot trial", memo, 1998 July 13.

6. Magnusen, P.E., Bucci, R.J., Hinkle, A.J., Brockenbrough, J.R., Konish, H.J., Miyasato, S. M., Final Report: The Role of Microstructure on the Fatigue Durability of Aluminum Aircraft Alloys, ONR Contract N00014-91-C-0128, Alcoa Technical Center, November 1995.

7. Magnusen, P.E., Bucci, R.J., Hinkle, A.J., Brockenbrough, J.R., Konish, H.J., Analysis and prediction of microstructural effects on long-term fatigue performance of an aluminum aerospace alloy, *Int. J. Fatigue*, Vol.19, Supp. No. 1, pp. S275 – S283, 1997.

8. Chu, M.G., "Solidification Characteristics of Commercial Aluminum Alloys Part 1: 7055, 7050, 7075, 2024," Alcoa Division Report 05-95-10M251, 1995 May 8.

9. Staley, J.T., "Influence of Microstructure on Fatigue and Fracture of Aluminum Alloys," International Symposium on Fracture Mechanics, George Washington University, Washington, D.C., September, 1978.

10. Alcoa-Davenport, IA, Plant trial data.

11. Helm, D., Gysler, A., Lutjering, G., Becker, J., and Fischer, G., In Light-Weight Alloys for Aerospace Applications, TMS (1989) 99-109.

12. Starke, Jr. E.A., Lutjering, G., Cyclic Plastic Deformation and Microstructure, in Fatigue and Microstructure, Metals Park: ASM (1978) 226-229.

13. Li, Ming & Butler Jr., John F., Non-dimensional microstructural parameters in intergranular fracture of aluminum alloys", *Proceedings of the Conference on the 70th Birthday of Dr. Owen Richmond*, Seven Springs, PA, October 19-20, 1998.

14. Personal conversations with Paul Baggethun.

15. Tokaji, K., Bian, J., Ogawa, T., Nakajima, M., "The microstructure dependence of fatigue behavior in Ti-15Mo-5Zr-3Al alloy," *Mat. Sci. and Eng*., Vol.A213, 1996, pp. 86-92.

16. Welpmann, K., Gysler, A., Lutjering, G., "Influence of Processing Related Variations of Grain Structure and Texture on Mechanical Properties of 7475" in Seventh International Light Metal Congress, Leoben/Vienna, 1981 June 22-26, Aluminium-Verlag GmbH, Dusseldorf, West Germany, pp. 158-159, 1981.

17. Miller, J.L., Fricke, W.G., "Fatigue Properties of Recrystallized and Unrecrystallized 6061-T6 Rotor Blade Extrusions," Alcoa Division Report 9-63-29/13-KF19, 1963 June 28.

18. Knorr, D.B., Weiland, H., "Practical Applications in Texture Analysis", *Journal of Metals*, Vol. 46, No. 9, September 1994, p. 31.

19. Knorr, D.B., Weiland, H., Szpunar, J.A., "Applying Texture Analysis to Materials Engineering Problems", *Journal of Metals*, Vol. 46, No. 9, September 1994, p. 32-36.

20. Teichman, M.M., Micro-Hardness of Particles in 7055 Alloy by Nanoindentation, internal Alcoa report, 2002 October 3.